Fusion of Remote Vision and On-Board Acceleration Data for the Vibration Estimation of Large Space Structures

by

Amy M. Bilton

Bachelor of Applied Science with Honors, Engineering Science
University of Toronto, 2004

Submitted to the Department of Aeronautics and Astronautics
in Partial Fulfillment of the Requirements for the Degree of
Master of Science in Aeronautics and Astronautics
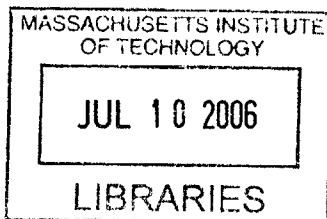
at the

Massachusetts Institute of Technology

June 2006

Signature of Author . . . .
Department of Aeronautics and Astronautics
May 9, 2006

Certified by . . . .
Steven Dubowsky
Professor of Mechanical Engineering
Thesis Supervisor

Accepted by . . . .
Jaime Peraire
Professor of Aeronautics and Astronautics
Chair, Committee on Graduate Studies

AERO

Fusion of Remote Vision and On-Board Acceleration Data for the Vibration Estimation of Large Space Structures

by

Amy M. Bilton

Submitted to the Department of Aeronautics and Astronautics
on May 9, 2006 in Partial Fulfillment
of the Requirements for the Degree of
Master of Science in Aeronautics and Astronautics

ABSTRACT

Future space structures such as solar power stations and telescopes are expected to be very large. These structures will require on-orbit construction. Due to the risks and costs of human extravehicular work, teams of robots will be essential for the on-orbit assembly of the large space structures. There are a number of technical challenges presented by such robotic construction. The structures will need to be made of lightweight materials and will be very flexible. Autonomous robots will require information about the vibrations of the flexible structures and their dynamic parameters in order to perform the construction efficiently. Often models of the structures are imperfect, therefore the magnitude of the vibrations of the structure must be estimated on-orbit.

This thesis presents a method for estimating the shape and dynamic parameters of a vibrating large space structure. This technique is a cooperative sensing approach using remote free-flying robot observers equipped with vision sensors and structure-mounted accelerometers. This approach exploits the complementary nature of the two types of sensors. Vision sensors are able to measure structure deflections at a high spatial frequency but are bandwidth limited. Accelerometers are able to make measurements at high temporal frequency, but are sparsely located on the structure.

The fused estimation occurs in three steps. First, the vision data is condensed in a modal decomposition that results in coarse estimates of modal coefficients. In the second step, the coarse estimates of the modal coefficients obtained from vision data are fused with the accelerometer measurements in a multi-rate nonlinear Kalman filter, resulting in a refined estimate of the modal coefficients and dynamic properties of the structure. In the final step, the estimated modal coefficients are combined with the mode shapes to provide a shape estimate of the entire structure.

Simulation and experimental results demonstrate that the performance of this fused estimation approach is superior to the performance achieved when using only a single type of sensor.

Thesis Supervisor: Steven Dubowsky, Professor of Mechanical Engineering

ACKNOWLEDGEMENTS

CONTENTS

FIGURES

TABLES

1

INTRODUCTION

1.1 Background

The energy needs of the earth are constantly increasing. Currently, the majority of earth's power is produced by burning fossil fuels. Not only is this process harmful to the environment, but also the supply of these fossil fuels is limited. This limited supply has lead many nations to become politically dependent on unstable areas of the world. In the future, the earth will need to utilize alternative energy sources to satisfy the increasing demand.

Space Solar Power Stations (SSPS) are emerging as a promising concept to provide earth with clean, environmentally friendly, renewable energy. Several designs for SPSS have been proposed including NASA's Sun Tower [27] (see Figure 1.1) and JAXA's Space Solar Power System [31, 36, 42] (see Figure 1.2). Both of these solar power stations use very large mirrors (dimensions on the order of several kilometers) to collect solar radiation. The radiation is then converted to electric power and is transmitted back to earth using microwaves or laser beams.

These structures will be orders of magnitude larger than current space structures such as the International Space Station. Due to their size, these structures will require on-orbit assembly. Human extravehicular activity (EVA) is too expensive and dangerous to complete such a mission. The construction of the SPSS will involve many repetitive

tasks and take a considerable amount of time. The use of robot teams will be essential to for the on-orbit construction of these large space structures [9, 26, 27, 31, 36, 37, 42].
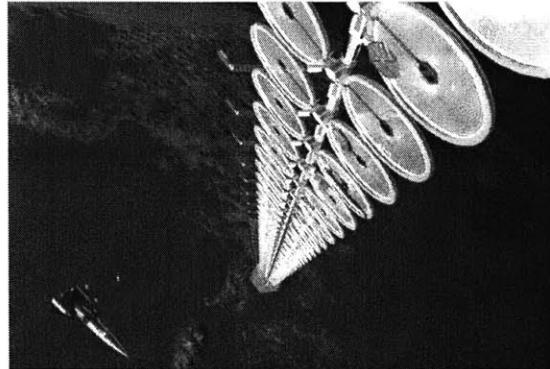
Figure 1.1. NASA's Sun Tower concept [27].
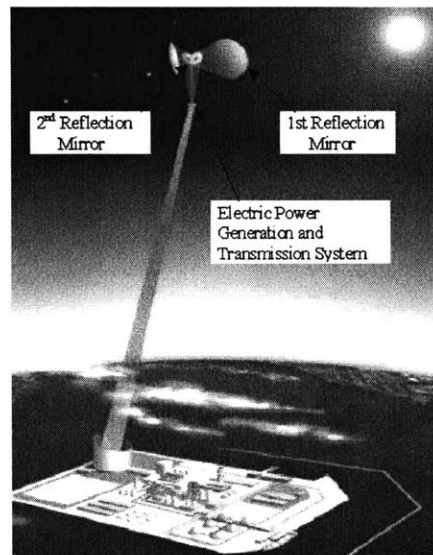
Figure 1.2. 2001 Baseline model of JAXA's 1GW experimental SSPS [36].

It has been proposed that this large space structure (LSS) construction consist of three main phases. In the first phase, LSS substructure modules are deployed from a launch vehicle. In the second phase, these modules are maneuvered to the close proximity of the main LSS by a team of free-flying robots (see Figure 1.3). In the final phase, the module is assembled into the main LSS by a team of manipulators likely

mounted on the LSS itself (see Figure 1.4). Once the LSS construction has been completed, robots will also be required to monitor the structures and conduct any necessary maintenance [31, 36, 42].
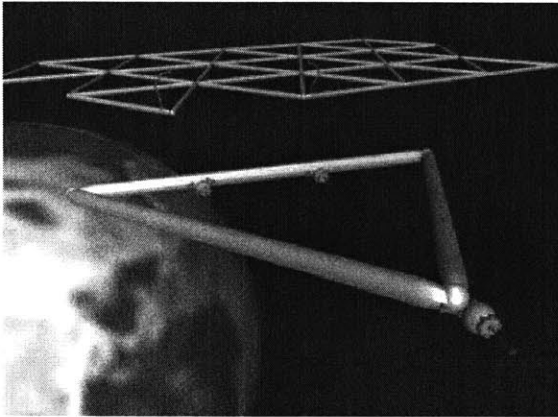
Figure 1.3. Transportation of a LSS by a team of free-flying robots [40].
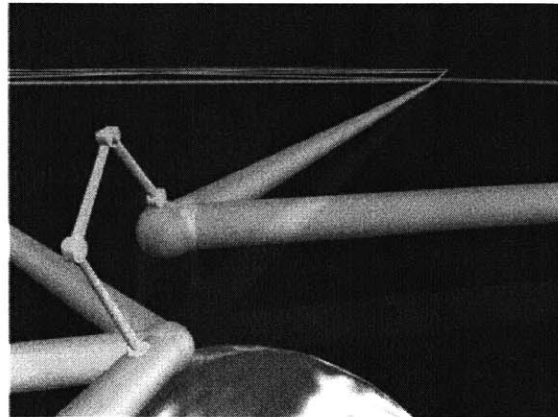
Figure 1.4. Assembly of LSS by robots mounted on then main LSS [40].

There are a number of technical challenges associated with such robotic construction. Space structures need to be made of lightweight materials and will be highly flexible with very low damping and natural frequencies. It is important that vibrations be controlled during the structure's transportation and assembly in order to prevent damage to both the structure and the robots.

In order for the transportation or assembly robots to control the vibrations, they will require knowledge of the structure's dynamic state (the modal coefficients) and the structural model (modal frequencies, modal damping, etc.) [13, 42]. It is highly unlikely that the structural model will be known exactly a priori and the robots will be unable to accurately compute the structure's dynamic state. Therefore, a critical technology for the autonomous construction of a large space structure is the on-orbit estimation of the structure and its components dynamic state, shape and dynamic parameters.

This thesis will explore using remote vision sensors and structure-mounted accelerometers together in concert to estimate the shape and dynamic parameters of a vibrating large space structure.

1.2 Literature Review

The problem addressed by this thesis is the estimation of the shape and dynamic parameters of a vibrating large space structure using remote vision sensors and structure-mounted accelerometers. This section presents a review of literature related to this problem.

1.2.1 Large Space Structure Vibration Estimation

The shape and dynamic parameter estimation of large space structures has been a topic of extensive research. In [45], Williams uses a matrix factorization method to estimate the mass matrix for a flexible structure. This mass matrix can then be used to refine estimates of the mode shapes, frequencies, and modal damping. In [14], Juang and Pappa use and Eigensystem Realization Algorithm to estimate the mass and stiffness matrices for a flexible system. While these methods may be useful for refining a model of a flexible space structure, they do not allow the estimation of the current state of the flexible structure.

Recently, the Kalman filter has been considered as a technique for estimating the vibration of a large space structure. Chen developed a Kalman filter to estimate both the parameters and state for a vibrating large space structure [7]. However, this technique failed to consider sensor limitations. This Kalman filter technique has been applied to structure mounted sensors by Lively et al [24] and to remote-vision sensors by Lichter

---

and Dubowsky [19, 20, 21]. The benefits of fusing data from these two types of sensors have not been examined.

1.2.2 Structure-Mounted Sensors

Many researchers have examined the use of on-board sensors, such as accelerometers, strain gauges, etc., to measure the vibrations of a flexible structure [3, 4, 11, 12, 17, 22, 24, 25, 34, 38, 47]. These sensors provide measurements at high frequencies, but can only be located at discrete points along the structure. As a result, a large number of structure-mounted sensors may be required to accurately estimate the shape of a vibrating structure. Such a large sensor array would require extensive and complex cabling, power supplies, electronics, etc. that would increase cost and weight and reduce reliability.

In addition, the placement of on-board sensors plays a large role in ability to accurately estimate the parameters of a vibrating large space structure. This area has been a topic of a large amount of research. Most of the methods developed use a metric of the observability of the desired modes. In [38], Tongco and Meldrum use the determinate of the Modal Correlation matrix as the metric to compare different on-board sensor configurations. This is also known as the D-optimality criteria. This technique maximizes the observability of the desired modes while ensuring very little spatial aliasing. However, this technique requires the evaluation of the condition number of the modal correlation matrix for all possible sensor configurations. Many techniques, such as genetic algorithms, have been considered to ease this computation [17, 43].

A second approach, considered by Gawronski, ranks each sensor location based on the observability grammian for all the modes of interest [11]. Then, the correlation between each candidate sensor location is calculated and the top ranked uncorrelated candidate locations are chosen. This method is more computationally efficient, as it only

requires a single set of computations for each candidate sensor location. This method also achieves similar results to the method mentioned previously.

1.2.3 Remote Vision Sensing

Vision sensors have also been considered as a method of estimating the vibrations of a flexible structure. In [29], Metaxas and Terzopoulis developed a technique to estimate the shape of a general deformable structure using a sequence of range images. This technique starts with a detailed mesh of the undeformed target. The moving target then provides a sequence of overlapping meshes. These are stitched together online using a Kalman filter. While this technique works well for terrestrial applications, the algorithm is computationally intensive and would be difficult to implement on space-qualified computers.

In [39], Tse and Heppler use a priori knowledge of the structures mode shapes to estimate the shape of a large flexible satellite. At each time-step, the range image data goes through a modal decomposition to yield an estimate of the modal coefficients. This method fails to use the knowledge of the dynamics of the system and the results from the previous measurements. This method can also result in the aliasing of higher frequency modes.

Lichter and Dubowsky [19, 20, 21] use a similar approach to the one mentioned above. This approach uses a priori knowledge of the structures mode shapes and dynamic model to estimate the shape and parameters of a vibrating large space structure. Similar to above, at each time-step, the range image undergoes a modal decomposition to yield a coarse estimate of the modal coefficients. These coarse estimates are then processed by a Kalman filter to achieve a refined estimate of the structures modal coefficients and dynamic parameters. In the final step, modal coefficients are combined with the mode shapes to estimate the final shape of the structure.

Vision sensors offer some advantages over structure-mounted sensors. Vision sensors can capture dense spatial deflection information for the flexible space structure, but are bandwidth limited. Also, range images are noisy, and data may be missing from large regions due to obfuscation. The harsh lighting conditions of space are often a problem for many vision sensors.

1.2.4 Multirate Fusion Techniques

A potentially advantageous approach would be to use the remote vision and on-board acceleration data in concert. The high spatial frequency provided by the vision system is complementary to the high temporal frequency provided by the structure-mounted sensors. One of the challenges associated with this approach is the two sample rates associated with the different types of sensors.

The fusion of measurements with different sample rates is a problem that has been well studied in literature. In [1], Andrisani and Gau use of two parallel Kalman filters to fuse measurements taken at different sample rates. One filter processes the fast rate measurement, the other processes the residual from the residuals from the first filter along with the slow rate measurement. The final estimate is achieved by blending the results from the two filters.

Several simpler approaches use only one Kalman filter to fuse the measurements. Niwa et al [30] use a single Kalman filter with a single set of state and measurement equations. The measurement covariance is changed to reflect the measurements available at a particular time-step. If a particular measurement is unavailable, the corresponding measurement covariance is set to infinity. Chroust and Vincze use a similar approach [2, 8]. A Kalman filter is implemented with a single set of state equations and two different measurement models. When a measurement is made, the state is predicted using the system model and the appropriate measurement model is applied to yield the current

estimate. This technique has been applied here to address the issue of two different sensor sample rates.

1.3 Problem Statement

This thesis develops a technique to use both remote vision sensors and structure-mounted accelerometers together in concert to estimate the shape and dynamic parameters of a vibrating large space structure. This technique exploits the complementary nature of these sensors. Structure-mounted accelerometers can be sampled a high rate, but a large number of sensors would be required to achieve an accurate state estimate. Vision sensors measure points with a high spatial frequency, but have a low sample rate and are unable to estimate the high frequency vibrations. This thesis will show that using these two types of measurements together makes it possible to achieve an accurate estimate of the structures state with a limited number of on-board sensors and low vision sample rate.

1.4 Thesis Organization

This thesis contains five chapters. This chapter presents the motivation and relevant background literature for this work. Chapter 2 develops the estimation architecture for large space structures by fusing measurements made by range imagers and structure-mounted accelerometers. In Chapter 3, the estimation technique is evaluated in simulation three different cases: a one-dimensional space structure, a three-dimensional space structure, and a space structure being manipulated by free flying robots. In Chapter 4, this estimation technique is tested experimentally on the Robotic Team Interactive Microgravity System in the MIT Field and Space Robotics Laboratory.

The final chapter summarizes the results of this thesis and makes recommendations for future work in this area.

2

ESTIMATOR STRUCTURE

2.1 Problem Statement and Assumptions

This thesis explores the use of remote vision sensors and structure-mounted accelerometers together in concert to estimate the shape and dynamic parameters of a vibrating large space structure. Robots can utilize these values during the construction of a large space structure. This section presents the assumptions made during the development of this work.

2.1.1 Structure Assumptions

It is assumed that the structure's dynamics are linear or weakly non-linear. In addition, it is assumed that the mode shapes of structure are known approximately a priori. In practice, these could be found using Finite-Element Methods (FEM) or on-ground testing. It is also assumed that the modal frequencies are known to with ± 20 percent. The estimator is able to perform well within this range and refine the estimate to the actual modal frequencies.

2.1.2 Sensor Assumptions

In this work it is assumed that there are two different types of sensors, remote vision sensors and structure-mounted accelerometers. The structure-mounted sensors used in the following development are accelerometers, but this method can be extended

to other types of sensor such as strain gauges. Accelerometers are assumed to be synchronous so that all the acceleration measurements are taken at approximately the same time. Also, accelerometer measurements are assumed to be noisy. The noise is assumed to be additive, white, unbiased and roughly Gaussian.

It is assumed that the vision sensors are synchronous and capture their data at the same time. It is also assumed that the relative time between samplings between vision and acceleration measurements is known. Further, it is assumed that the vision measurements are noisy, and that the noise is additive, white, unbiased and roughly Gaussian in all 3 coordinates (x, y, and z).

It is also assumed that force sensors will measure the external forces and torques that are applied to the structure by control robots. Similar to the previous sensors, it is assumed that these measurements will be noisy. The noise is assumed to be additive, white, unbiased and roughly Gaussian.

2.2 Estimation Architecture

As stated above, this thesis considers the use of both low-frequency remote-vision sensors and high-frequency structure-mounted accelerometers to estimate the shape and dynamic parameters of a vibrating large space structure. The architecture developed in this thesis is an extension of work done by Dr. Matthew Lichter [21]. Lichter developed architecture to estimate the state, shape and modal parameters of a large space structure based on a sequence of range images. This thesis considers the addition of accelerometers to this architecture, as well as the incorporation of well-known external forces.

The goal is to estimate the modal coefficients, $q_i(t)$, their derivatives, $\dot{q}_i(t)$, the modal frequencies, ω_i, and the modal damping coefficients, ζ_i for all of the modes of

interest. These values will be available for use in the feedback for a robot controller. The magnitude of the modal coefficients can also be used to obtain an estimate of the shape of the structure using simple modal reconstruction.

The estimation architecture used here is shown in Figure 2.1. The estimation occurs in three steps. First, the vision data is condensed in a modal decomposition that results in coarse estimates of modal coefficients, $\bar{q}_i(t)$. In the second step, the coarse estimates of the modal coefficients obtained from vision data are merged with the accelerometer measurements in a multi-rate nonlinear Kalman filter, resulting in a refined estimate of the modal coefficients, $\hat{q}_i(t)$. In the final step, the estimated modal coefficients are combined with the mode shapes to give the structure a final shape. This chapter will now detail these steps.
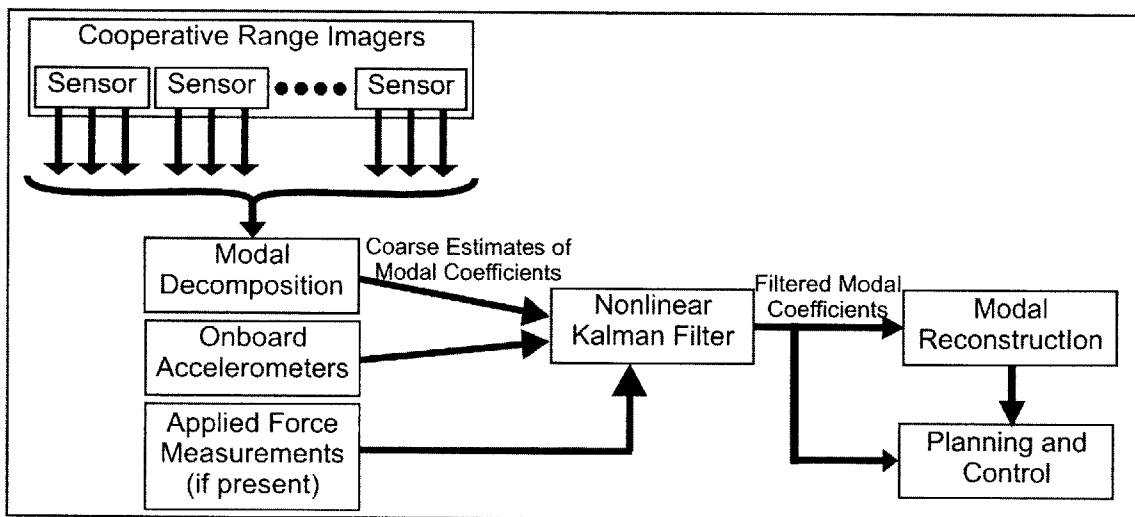
Figure 2.1. Estimation architecture.

2.3 Modal Decomposition

2.3.1 Vision Sensors

As shown in Figure 2.1, the first step in the estimation process is a modal decomposition. In this step, a large amount of pixel-level information is condensed into a small number of coarse estimates of the modal coefficients, $\tilde{q}_i(t)$. The modal decomposition of vision sensors is fully outlined in [21]. This thesis will highlight the main aspects of the derivation. The vision sensors measure the deflection of the structure. These deflections relate to the modal coefficients by:

$$z(x,t) = \sum_{i=1}^{m} \phi_i(x) q_i(t) \tag{2.1}$$

where $q_i(t)$ represents the ith modal coefficient and $\phi_i(x)$ represents the ith mode shape.

The vision sensors will make measurements in a discrete sample space $Y \subset S$, where S is the continuous space in which all possible measurements will lie. The sample space Y will be time varying.

The inner product of the mode shapes over this discrete sample space is a simple summation given by:

$$\left\langle \Phi_i, \Phi_j \right\rangle_y = \sum_{k=1}^{n} \phi_i(y_k) \phi_j(y_k)$$

where y_k is the kth sample point, and n is the total number of sample points in the sample space Y.

The modal correlation matrix, M_y is a matrix containing the inner products between m excited modes as defined in the discrete sample space Y. It is given by:

$$M_y = \langle \Phi, \Phi \rangle_y = \Phi^T \Phi = \begin{bmatrix} \langle \Phi_1, \Phi_1 \rangle_y & \cdots & \langle \Phi_1, \Phi_i \rangle_y & \cdots & \langle \Phi_1, \Phi_m \rangle_y \\ \vdots & \ddots & \vdots & \ddots & \vdots \\ \langle \Phi_i, \Phi_1 \rangle_y & \cdots & \langle \Phi_i, \Phi_i \rangle_y & \cdots & \langle \Phi_i, \Phi_m \rangle_y \\ \vdots & \ddots & \vdots & \ddots & \vdots \\ \langle \Phi_m, \Phi_1 \rangle_y & \cdots & \langle \Phi_m, \Phi_i \rangle_y & \cdots & \langle \Phi_m, \Phi_m \rangle_y \end{bmatrix} \quad (2.2)$$

where Φ is a matrix whose m-columns are composed of the first m mode shapes of the structure.

The modal correlation matrix guaranteed to be positive semi-definite. The semi-definite condition arises when some of the modes are unobservable or spatially aliased. For the remainder of this derivation it is assumed that M_y is positive definite, well-conditioned and invertible.

Using the modal correlation matrix, we can relate the modal coefficients directly to the deflections that will be measured by the vision sensors. Rewriting equation (2.1) in vector form gives:

$$z = \Phi q$$

then multiplying both sides of the equation by Φ^T

$$\Phi^T z = \Phi^T \Phi q$$
$$\Rightarrow \langle \Phi, z \rangle_y = M_y q \quad (2.3)$$
$$\Rightarrow q = M_y^{-1} \langle \Phi, z \rangle_y$$

The measurements made by the remote vision sensors will be noisy. These measurements can be expressed as:

$$\begin{Bmatrix} \overline{z}(y_1,t) \\ \vdots \\ \overline{z}(y_k,t) \\ \vdots \\ \overline{z}(y_n,t) \end{Bmatrix} = \begin{Bmatrix} z(y_1,t) \\ \vdots \\ z(y_k,t) \\ \vdots \\ z(y_n,t) \end{Bmatrix} + \begin{Bmatrix} e_1 \\ \vdots \\ e_k \\ \vdots \\ e_n \end{Bmatrix}$$

where $z(y_k,t)$ is the true deformation at point y_k and e_k is the measurement error at point y_k. Rewriting this equation in vector form gives:

$$\overline{\mathbf{z}} = \mathbf{z} + \mathbf{e}$$

Therefore the coarse estimates of the modal coefficients can be written using equation 2.3 as follows:

$$\begin{aligned}
\breve{\mathbf{q}}(t) &= \mathbf{M}_y^{-1}\langle \boldsymbol{\Phi}, \overline{\mathbf{z}} \rangle_y \\
&= \mathbf{M}_y^{-1}\langle \boldsymbol{\Phi}, \mathbf{z} \rangle_y + \mathbf{M}_y^{-1}\langle \boldsymbol{\Phi}, \mathbf{e} \rangle_y \\
&= \mathbf{q}(t) + \mathbf{M}_y^{-1}\langle \boldsymbol{\Phi}, \mathbf{e} \rangle_y \\
&= \mathbf{q}(t) + \mathbf{w}_v(t)
\end{aligned} \qquad (2.4)$$

Since $\mathbf{e}$ is unbiased, the expected value of the error in the coarse estimate $\breve{\mathbf{q}}(t)$ based on remote vision measurements can be written as:

$$\begin{aligned}
E[\mathbf{w}_v(t)] &= E[\mathbf{q}(t) - \breve{\mathbf{q}}(t)] \\
&= E\left[\mathbf{M}_y^{-1}\langle \boldsymbol{\Phi}, \mathbf{e} \rangle_y\right] \\
&= 0
\end{aligned}$$

Therefore, $\breve{\mathbf{q}}(t)$ provides an unbiased estimate of the modal coefficients.

The error covariance on the coarse estimates formed from the vision measurements can be derived as follows.

$$
\begin{aligned}
A_{vv} &= E\left[\mathbf{w}_v(t)\mathbf{w}_v(t)^T\right] \\
&= E\left[\mathbf{M}_y^{-1}\langle\Phi,\mathbf{e}\rangle_y\left(\mathbf{M}_y^{-1}\langle\Phi,\mathbf{e}\rangle_y\right)^T\right]
\end{aligned}
$$

Substituting in the definition of the inner product gives:

$$
\begin{aligned}
A_{vv} &= \mathbf{M}_y^{-1}E\left[\Phi^T\mathbf{e}\mathbf{e}^T\Phi\right]\mathbf{M}_y^{-1} \\
&= \mathbf{M}_y^{-1}\Phi^T\sigma_v^2 I\Phi\mathbf{M}_y^{-1}
\end{aligned}
$$

where σ_v^2 is the variance in the vision sensor measurements. Simplifying the above equation gives the final vision measurement error covariance.

$$
\begin{aligned}
A_{vv} &= \sigma_v^2\mathbf{M}_y^{-1}\mathbf{M}_y\mathbf{M}_y^{-1} \\
&= \sigma_v^2\mathbf{M}_y^{-1}
\end{aligned}
\tag{2.5}
$$

2.3.2 Accelerometers

In the general case, acceleration measurements do not undergo a modal decomposition. These measurements are dependent on the modal frequencies and damping, values that will be uncertain and will need to be estimated. Also, the accelerometers produce a small amount of information at each time step when compared to the vision system. Therefore, the additional computation required will be negligible.

The acceleration can be defined at any point on the structure using:

$$\ddot{z}(x,t) = \sum_{i=1}^{m} \phi_i(x)\ddot{q}_i(t) = \mathbf{\Phi}(x)\ddot{\mathbf{q}}(t) \qquad (2.6)$$

where the unforced dynamics of $q(t)$ are given by:

$$\ddot{q}_i(t) = -\omega_i^2 q_i(t) - 2\zeta_i \omega_i \dot{q}_i(t)$$

where ζ_i is the ith modal damping coefficient and ω_i is the ith natural frequency.

The acceleration measurements are made in a time-invariant sample space $X \subset S$. These acceleration measurements can be written as:

$$\begin{Bmatrix} \overline{\ddot{z}}(x_1,t) \\ \vdots \\ \overline{\ddot{z}}(x_k,t) \\ \vdots \\ \overline{\ddot{z}}(x_n,t) \end{Bmatrix} = \begin{Bmatrix} \ddot{z}(x_1,t) \\ \vdots \\ \ddot{z}(x_k,t) \\ \vdots \\ \ddot{z}(x_n,t) \end{Bmatrix} + \begin{Bmatrix} e_{a,1} \\ \vdots \\ e_{a,k} \\ \vdots \\ e_{a,n} \end{Bmatrix}$$

where $\ddot{z}(x_k,t)$ is the true acceleration at sample point x_k, $\overline{\ddot{z}}(x_k,t)$ is the measured acceleration at x_k, $e_{a,k}$ is the accelerometer measurement noise at x_k, and n is the number of accelerometers mounted on the flexible structure. Rewriting this equation in vector form gives:

$$\overline{\ddot{\mathbf{z}}} = \ddot{\mathbf{z}} + \mathbf{e}_\mathbf{a}$$

Error covariance for the accelerometers in the general case is given by:

$$A_{aa} = E\left[(\bar{\ddot{z}} - \ddot{z})(\bar{\ddot{z}} - \ddot{z})^T\right]$$
$$= E\left[e_a e_a^T\right] \tag{2.7}$$
$$= \sigma_a^2 I_n$$

where σ_a^2 is the variance on the accelerometer measurements. It is assumed that all accelerometers have the same measurement variance.

In the special case that you have a good knowledge of the modal frequencies of the structure and very light damping, it is possible to perform a modal decomposition on the acceleration measurements. This case is presented in full detail in Appendix A.

2.4 Kalman Filter

The next step in the estimation process is a sinusoid estimator. In this step, the low-frequency coarse estimates of the modal coefficients from the vision data, $\breve{q}(t)$, and the high-frequency acceleration measurements, $\bar{\ddot{z}}$, are fused together to form an estimate of the actual modal coefficients, $\hat{q}(t)$. Also, it is advantageous to refine the estimate of the modal frequencies, ω, and modal damping coefficients, ζ. In order to allow for a fast-online implementation, a Kalman filter is used.

The Kalman filter is a predictor-corrector method. It uses a process model to project the current state forward till a measurement is taken. Once a measurement is made, it uses the second order characteristics of the process and measurement noise to provide an updated estimate.

The process model can be derived as follows. The modal coefficients can be written as damped sinusoids of the following form:

$$q_i(t) = q_i(0)exp(-\zeta_i\omega_it)sin(\omega_it + \varphi_i)$$

where $q_i(0)$ is the initial value of the ith modal coefficient, φ_i is the phase of the ith mode. Differentiating twice gives the continuous-time process model.

$$\frac{d}{dt}\begin{Bmatrix} q_i(t) \\ \dot{q}_i(t) \\ \omega_i \\ \zeta_i \end{Bmatrix} = \begin{Bmatrix} \dot{q}(t) \\ -\omega_i^2 q_i(t) - 2\zeta_i \omega_i \dot{q}_i(t) \\ 0 \\ 0 \end{Bmatrix} + v_i \qquad (2.8)\text{a}$$

Note the independence on the phase. When expressed in discrete-time with time step Δt, the process model becomes:

$$\begin{Bmatrix} q_i \\ \dot{q}_i \\ \omega_i \\ \zeta_i \end{Bmatrix}_{(t+\Delta t)} = \begin{Bmatrix} exp(-\zeta_i \omega_i \Delta t)\left(q_i \cos(\omega_{d,i} \Delta t) + \dfrac{\dot{q}_i + \zeta_i \omega_i q_i}{\omega_{d,i}} sin(\omega_{d,i} \Delta t) \right) \\ exp(-\zeta_i \omega_i \Delta t)\left(\dot{q}_i \cos(\omega_{d,i} \Delta t) - \dfrac{\zeta_i \omega_i \dot{q}_i + \omega_i^2 q_i}{\omega_{d,i}} sin(\omega_{d,i} \Delta t) \right) \\ \omega_i \\ \zeta_i \end{Bmatrix}_{(t)} + v_i \qquad (2.8)\text{b}$$

where $\omega_{d,i}$ is the ith damped natural frequency as given by:

$$\omega_{d,i} = \omega_i \sqrt{1 - \zeta_i^2}$$

The derivation of the discrete-time process model is detailed in Appendix C. Well-known applied forces, from control robots for example, can also be incorporated into this process model. This case is presented in Section 2.6.

The process noise is represented by $v = \{v_q \quad v_{\dot{q}} \quad v_\omega \quad v_\zeta\}^T$ and it is characterized by the covariance matrix:

$$\Lambda_{vv} = E\left[vv^T \right] \tag{2.9}$$

The values of the entries in this matrix should be chosen to represent the uncertainty in the dynamic model. These uncertainties could be caused by unmodeled effects such as gravity gradient, solar pressure, orbital dynamics, structural non-linearity, etc.

A multi-rate Kalman filter is used to fuse together the low-frequency coarse modal coefficients formed using the vision measurements and the high-frequency acceleration measurements. The filter must be able to accommodate the different sensor sample rates. In order to do this, the filter uses two separate measurement models. The state vector is projected forward until a measurement is available, then the appropriate update model is applied. This method is depicted in Figure 2.2.
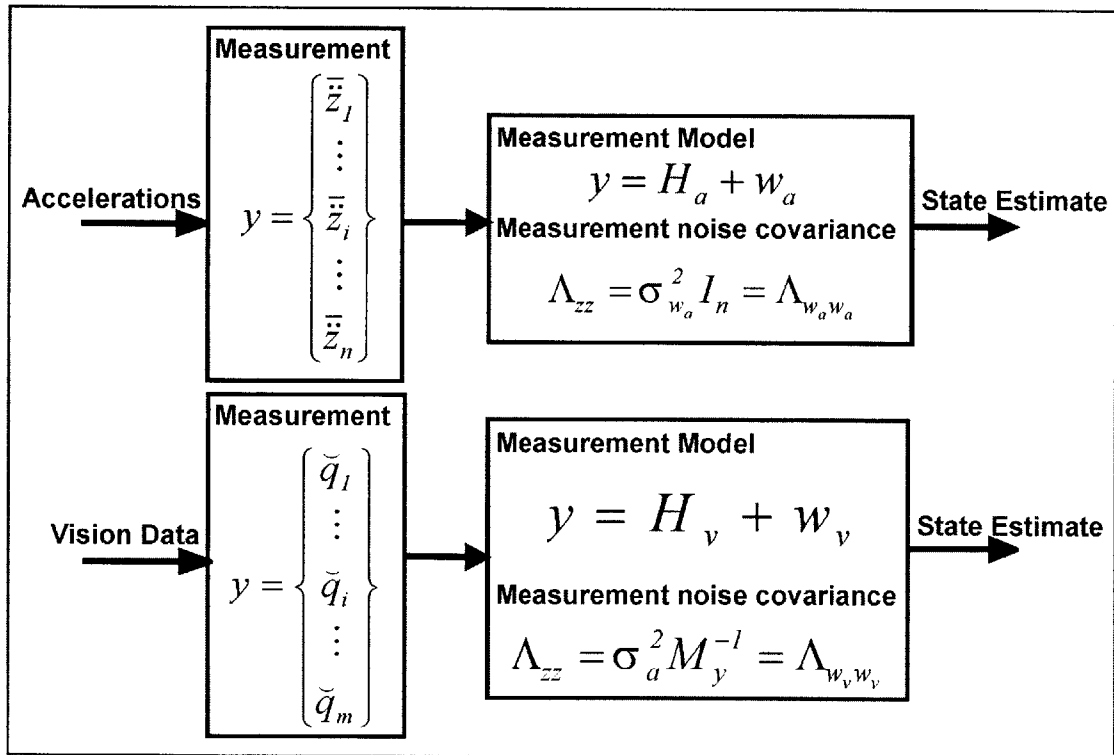
Figure 2.2. Multi-rate update models.

The vision-based measurements provide a coarse estimate of modal coefficients, $\bar{q}(t)$, to the Kalman filter. In this case the measurement model is simply

$$y = \left\{ \begin{array}{c} q_1 \\ \vdots \\ q_i \\ \vdots \\ q_m \end{array} \right\} + \left\{ \begin{array}{c} w_{v,1} \\ \vdots \\ w_{v,i} \\ \vdots \\ w_{v,m} \end{array} \right\} = H_v + w_v \tag{2.10}$$

The accelerometers provide acceleration measurements directly to the Kalman filter. The measurement model for the accelerometers using equation 2.6 is given by:

$$\left\{ \begin{array}{c} \ddot{z}(x_1,t) \\ \vdots \\ \ddot{z}(x_k,t) \\ \vdots \\ \ddot{z}(x_n,t) \end{array} \right\} = \left\{ \begin{array}{c} \sum_{i=1}^{m} (-\omega_i^2 q_i(t) - 2\zeta_i\omega_i\dot{q}_i(t))\phi_i(x_1) \\ \vdots \\ \sum_{i=1}^{m} (-\omega_i^2 q_i(t) - 2\zeta_i\omega_i\dot{q}_i(t))\phi_i(x_k) \\ \vdots \\ \sum_{i=1}^{m} (-\omega_i^2 q_i(t) - 2\zeta_i\omega_i\dot{q}_i(t))\phi_i(x_n) \end{array} \right\} + \left\{ \begin{array}{c} e_{a1} \\ \vdots \\ e_{ak} \\ \vdots \\ e_{an} \end{array} \right\} \tag{2.11}$$

$$= H_a + w_a$$

This implementation allows the Kalman filter to fuse the information in a statistically optimal way. Any time a measurement is observed, the Kalman filter determines how much to weight the measurement based on the statistical properties of the measurement model and the current state covariance. Therefore, if one of the measurements is much noisier than the other, the Kalman filter will apply only a very small weight to those measurements.

The final information required by the Kalman filter is an initial estimate of the state and its associated covariance. For the general case of a vibrating beam the initial state estimate is given by:

$$\begin{Bmatrix} \hat{q}(0) \\ \hat{\dot{q}}(0) \\ \hat{\omega}(0) \\ \hat{\zeta}(0) \end{Bmatrix} = \begin{Bmatrix} \breve{q}(0) \\ 0 \\ \omega_{exp} \\ \zeta_{exp} \end{Bmatrix} \tag{2.12}$$

where $\breve{q}(0)$ is the initial coarse vision estimate, and ω_{exp} and ζ_{exp} are the expected modal frequencies and damping.

The Kalman filter also requires knowledge of the uncertainty in the initial state estimate. The estimate error at any time t is represented by:

$$\theta(t) \equiv \begin{Bmatrix} \hat{q}(t) - q(t) \\ \hat{\dot{q}}(t) - \dot{q}(t) \\ \hat{\omega}(t) - \omega \\ \hat{\zeta}(t) - \zeta \end{Bmatrix}$$

The initial state error covariance is given by:

$$\Lambda_{\theta\theta}(0) \equiv E\left[\theta(t)\theta(t)^T\right]$$

$$= \begin{bmatrix} \Lambda_{ww} & & & \\ & E\left[\{\dot{q}(0)\}\{\dot{q}(0)\}^T\right] & & \\ & & E\left[\{\omega - \omega_{exp}\}\{\omega - \omega_{exp}\}^T\right] & \\ & & & E\left[\{\zeta - \zeta_{exp}\}\{\zeta - \zeta_{exp}\}^T\right] \end{bmatrix} \tag{2.13}$$

where Λ_{ww} is given by equation (2.5). The initial state covariance should be chosen to represent the uncertainty in the initial estimate.

The Kalman filter is now straightforward to implement using equations (2.4) through (2.13) and applying the appropriate update model as shown in Figure 2.2. The process model is non-linear, therefore a non-linear Kalman filter must be used [6]. In all the experiments and simulations presented in this thesis an Unscented Kalman filter [15] was used with good performance.

2.5 Modal Reconstruction

In this final step, an estimate of the structure's final shape is formed using the a priori knowledge of the mode shapes and the estimate of the modal coefficients, $\hat{q}_i(t)$, from the Kalman filter. This reconstruction can be represented by:

$$\hat{z}(x,t) = \sum_{i=1}^{m} \hat{\phi}_i(x)\hat{q}_i(t) = \hat{\Phi}(x)\hat{q}(t)$$ (2.14)

where $\hat{\Phi}(x)$ is a matrix whose columns are the approximate a priori mode shapes and $\hat{q}(t)$ is a column vector containing the estimated modal coefficients. The effects of the uncertainty in the mode shapes is discussed in Appendix B.

2.6 Known Applied Forces

If well-known external forces are applied to the flexible structure, from robotic systems for example, additional terms will need to be incorporated into the equations for the measurement and process models shown above. This case has not been discussed in

literature. In the presence of external forces, the dynamics of the modal coefficients become:

$$\ddot{q}_i(t) = \sum_{k=1}^{p} b_{ki} F_k(t) - \omega_i^2 q_i(t) - 2\zeta_i \omega_i \dot{q}_i(t) \qquad (2.15)$$

where b_{ki} is the magnitude of the ith mode shape at the kth actuator, and $F_k(t)$ is the force applied by the kth actuator and p is the total number of actuators.

It is assumed that the forces will be well known. In reality, this would be accomplished by a force sensor. Like all sensors, the measurements from the force sensor are assumed to be noisy. The measurements from the force sensor can be written as:

$$\begin{Bmatrix} \overline{F}_1(t) \\ \vdots \\ \overline{F}_k(t) \\ \vdots \\ \overline{F}_p(t) \end{Bmatrix} = \begin{Bmatrix} F_1(t) \\ \vdots \\ F_k(t) \\ \vdots \\ F_p(t) \end{Bmatrix} + \begin{Bmatrix} e_{F,1} \\ \vdots \\ e_{F,k} \\ \vdots \\ e_{F,p} \end{Bmatrix}$$

or in vector notation

$$\overline{F} = F + e_F$$

This noise will need to be incorporated into the process noise covariance and the acceleration measurement noise covariance.

Using equation (2.15), we can rewrite the continuous-time process model for the case of known applied forces as:

$$\frac{d}{dt}\begin{Bmatrix} q_i(t) \\ \dot{q}_i(t) \\ \omega_i \\ \zeta_i \end{Bmatrix} = \begin{Bmatrix} \dot{q}(t) \\ \sum_{k=1}^{p} b_{ki}F_k(t) - \omega_i^2 q_i(t) - 2\zeta_i\omega_i\dot{q}_i(t) \\ 0 \\ 0 \end{Bmatrix} + v_i \qquad (2.16)$$

or in discrete time

$$\begin{Bmatrix} q_i \\ \dot{q}_i \\ \omega_i \\ \zeta_i \end{Bmatrix}_{(t+\Delta)} = \begin{Bmatrix} exp(-\zeta_i\omega_i\Delta)\left(q_i\,cos(\omega_{d,i}\Delta) + \dfrac{\dot{q}_i + \zeta_i\omega_i q_i}{\omega_{d,i}}\,sin(\omega_{d,i}\Delta)\right) \\ exp(-\zeta_i\omega_i\Delta)\left(\dot{q}_i\,cos(\omega_{d,i}\Delta) - \dfrac{\zeta_i\omega_i\dot{q}_i + \omega_i^2 q_i}{\omega_{d,i}}\,sin(\omega_{d,i}\Delta)\right) \\ \omega_i \\ \zeta_i \end{Bmatrix}_{(t)}$$

$$+ \begin{Bmatrix} \sum_{k=1}^{p} b_{ki}\overline{F}_k\left(\dfrac{exp(-\zeta_i\omega_i\Delta)}{\omega_i^2}\left(-\dfrac{\omega_i}{\omega_{d,i}}\,sin(\omega_{d,i}\Delta) - cos(\omega_{d,i}\Delta)\right) + \dfrac{1}{\omega_i^2}\right) \\ \sum_{k=1}^{p} \dfrac{b_{ki}\overline{F}_k\,exp(-\zeta_i\omega_i\Delta)}{\omega_{d,i}}\,sin(\omega_{d,i}\Delta) \\ 0 \\ 0 \end{Bmatrix}_{(t)} + v_{iF} + v_{i0} \qquad (2.17)$$

where v_{i0} is the process noise due to unmodeled effects and v_{iF} is the process noise due to the noise in the applied force measurements, which is given by:

$$v_{iF} = \begin{Bmatrix} \sum_{k=1}^{p} b_{ki}e_{F,k}\left(\dfrac{exp(-\zeta_i\omega_i\Delta)}{\omega_i^2}\left(-\dfrac{\omega_i}{\omega_{d,i}}\,sin(\omega_{d,i}\Delta) - cos(\omega_{d,i}\Delta)\right) + \dfrac{1}{\omega_i^2}\right) \\ \sum_{k=1}^{p} \dfrac{b_{ki}e_{F,k}\,exp(-\zeta_i\omega_i\Delta)}{\omega_{d,i}}\,sin(\omega_{d,i}\Delta) \\ 0 \\ 0 \end{Bmatrix} \qquad (2.18)$$

The derivation of the discrete time process model is included in Appendix C. For the case of noisy applied forces the process noise covariance is defined as:

$$\Lambda_{vv} = \Lambda_{vv_0} + E\left[v_{iF}\, v_{iF}^T\right] \tag{2.19}$$

where Λ_{vv_0} is given by equation (2.6).

The modal decomposition and the measurement model for the vision-type sensors remain identical to the formulation shown in Section 2.3.1. However, the measurement model for the accelerometers becomes:

$$
\left\{
\begin{array}{c}
\ddot{z}(x_1,t)\\
\vdots\\
\ddot{z}(x_k,t)\\
\vdots\\
\ddot{z}(x_n,t)
\end{array}
\right\}
=
\left\{
\begin{array}{c}
\sum\limits_{i=1}^{m}(\sum\limits_{k=1}^{p} b_{ki}F_k(t) - \omega_i^2 q_i(t) - 2\zeta_i\omega_i\dot{q}_i(t))\phi_i(x_1)\\
\vdots\\
\sum\limits_{i=1}^{m}(\sum\limits_{k=1}^{p} b_{ki}F_k(t) - \omega_i^2 q_i(t) - 2\zeta_i\omega_i\dot{q}_i(t))\phi_i(x_k)\\
\vdots\\
\sum\limits_{i=1}^{m}(\sum\limits_{k=1}^{p} b_{ki}F_k(t) - \omega_i^2 q_i(t) - 2\zeta_i\omega_i\dot{q}_i(t))\phi_i(x_n)
\end{array}
\right\}
+
\left\{
\begin{array}{c}
e_{a1}\\
\vdots\\
e_{ak}\\
\vdots\\
e_{an}
\end{array}
\right\}
\tag{2.20}
$$

$$= \Phi(B\overline{F} - \Omega^2 q - 2Z\Omega\dot{q}) - \Phi Be_F + e_a$$

$$= H_a + w_a$$

The measurement noise covariance for the accelerometers in this case becomes:

$$
\begin{aligned}
\Lambda_{aa} &= E\left[(\ddot{\overline{z}} - \ddot{z})(\ddot{\overline{z}} - \ddot{z})^T\right]\\
&= E\left[e_a e_a^T\right]\\
&= \sigma_a^2 I_n
\end{aligned}
\tag{2.21}
$$

The implementation of the Kalman filter can now be implemented using equations (2.4) to (2.5) and (2.16) to (2.21) and applying the appropriate update model as shown in Figure 2.2. The implementation is identical to the case presented in Section 2.4.

CHAPTER

3

SIMULATION STUDIES

3.1 Introduction

This chapter presents simulation studies for the estimator discussed in the previous chapter. These simulations were conducted for three different cases: a one-dimensional space structure, a planar space structure, and in the feedback loop for a large space structure transportation controller. In all three cases, the performance of the estimator using the data from both the remote vision sensors and structure-mounted accelerometers is compared to the performance of the estimator when using only a single type of sensor.

3.2 One-Dimensional Space Structure

3.2.1 Simulation Model

Simulation studies were performed to evaluate the theoretical performance of this approach. A simulation environment was developed in MATLAB. The structure used in the one-dimensional simulations is shown in Figure 3.1. The beam is built from rods and cables and is considered an accurate representation of the modules that will be used in the construction of the space solar power systems. The structural properties were

provided from finite element analysis conducted by Dimitris Tzeranis.   A summary of
the structural properties is shown in Table 3.1.
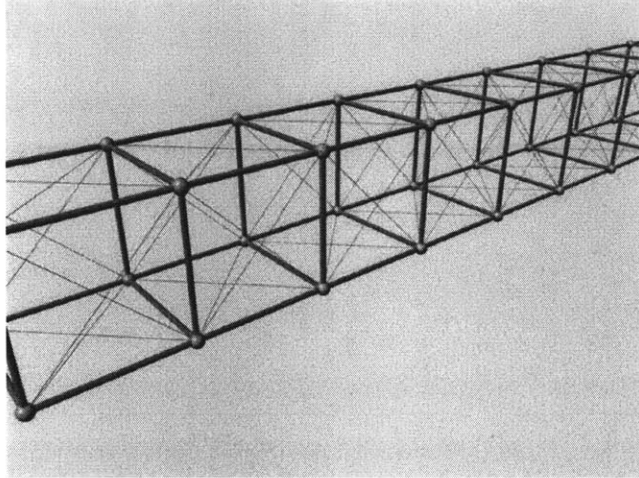
Figure 3.1. Flexible structure [40].

Table 3.1. Properties of flexible beam [40].

Parameters	Values
Mass	600 kg
Inertia	2×10^6 kgm^2
Dimensions	Length 200 m, Width 1m, Height 1 m
Stiffness	0.156 Gpa
Natural Frequencies	0.20, 0.55, 1.08, 1.78, 2.67, 3.75, 5.02 Hz

Simulated accelerometers were placed on the flexible structure.   These
accelerometers were sampled at a rate of 100 Hz and measure the acceleration
perpendicular to the beam.   Gaussian sensor noise was added to the acceleration
measurements with a standard deviation of 5% of the maximum acceleration.   Vision
measurements of the structure were also simulated.   It is assumed that one remote vision
sensor observes the entire vibrating structure from a distance of 100m, measuring

deflections at 40 locations. Gaussian sensor noise was also added to the vision measurements with a standard deviation of 0.5 m.

3.2.2 Estimator Performance

Simulations were performed to determine the performance of this fusion-based approach. These tests varied two parameters: the number of accelerometers mounted on the flexible beam and the sample rate of the vision sensor. The objective of the estimator is to provide an accurate estimate of the flexible beam's shape.

The error in the estimate at the end of the beam is used to compare different sensor configurations. It is important that the beam-ends be accurately estimated since these points are grasped by robots during the transportation and assembly phase of LSS construction. Here, the comparison metric is the time required for the beam-end estimate to converge within 5cm of the true value. This tolerance was chosen based on the size of robot grippers [9]. The estimate must converge within 10 seconds.

Each sensor configuration is tested against 20 different data sets in order to ensure independence on initial conditions. In each data set, all modes are vibrating with equal energy. The phase for each mode, φ_i, was randomly selected over the interval from 0 to 2π. A total of 14 modes were simulated, 8 of these modes were estimated.

Figure 3.2 shows the time required for a vision-based estimate to converge for various sample rates. The estimator is only able to meet the specification with a vision sample rate of 47 Hz or above. This sample rate is very substantial for such a simple element, particularly for space-qualified hardware.
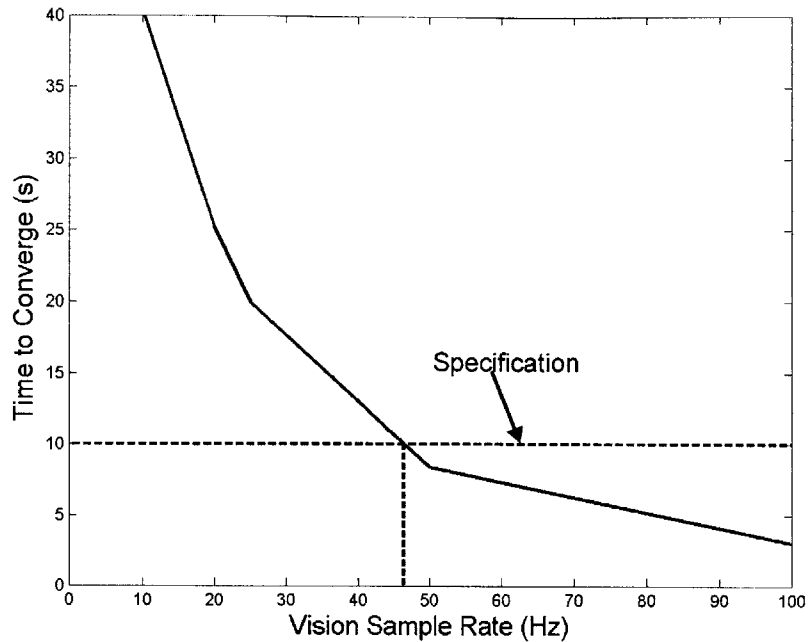
Figure 3.2. Convergence time of vision based estimates, 1-D large space structure.

Figure 3.3 shows the time required for the estimate to converge for different numbers of evenly spaced accelerometers. The estimator is only able to meet the specification with 25 accelerometers or more. The amount of infrastructure required for a single accelerometer makes this large number undesirable. Also note that the convergence time is not monotonically decreasing. This occurs due to the spacing of the accelerometers. In some of the configurations, spatially aliasing occurs and the performance of the estimator is degraded.
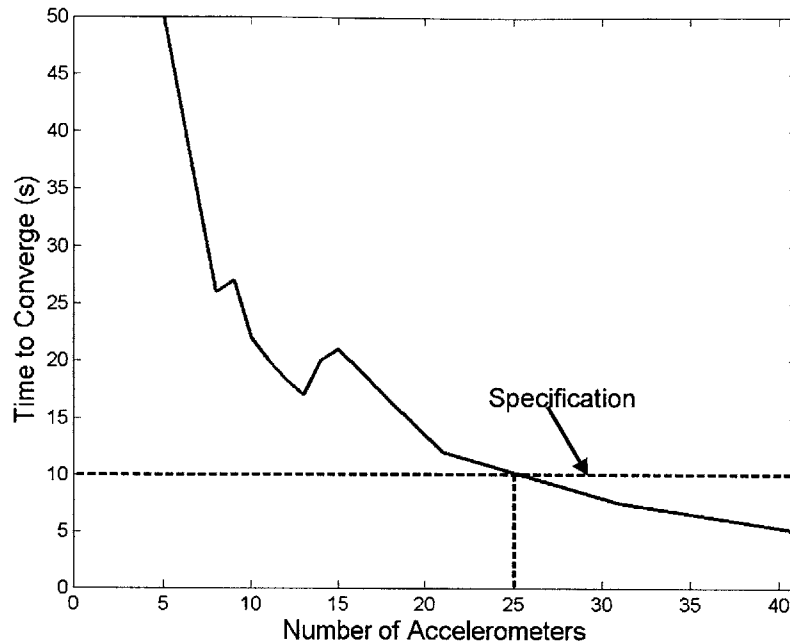
Figure 3.3. Convergence time for acceleration based estimates, evenly spaced accelerometers, 1-D large space structure, no rigid body motion.

A better approach is to place the sensors based on an observability metric as is described in Section 1.2.2. Both of the sensor placement algorithms discussed in Section 1.2.2 were implemented. For this simple beam, both methods yielded similar sensor locations. A sample optimal sensor configuration for 11 accelerometers, found using the D-Optimality criteria [38], is shown in Figure 3.4.
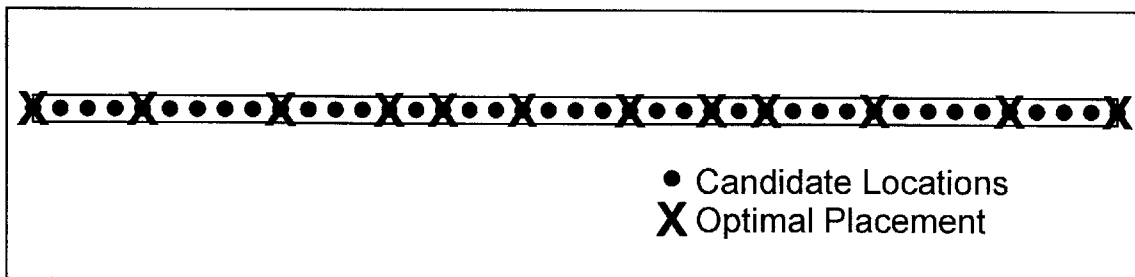
Figure 3.4. Optimal sensor placement for 11 accelerometers using D-Optimality criteria.

Figure 3.5 shows the time required for the estimate to converge when using measurements from optimally placed accelerometers. In this case, the convergence time is monotonically decreasing. In this case, 21 accelerometers are required to meet the desired specification. This number is relatively high for such a simple structural element.
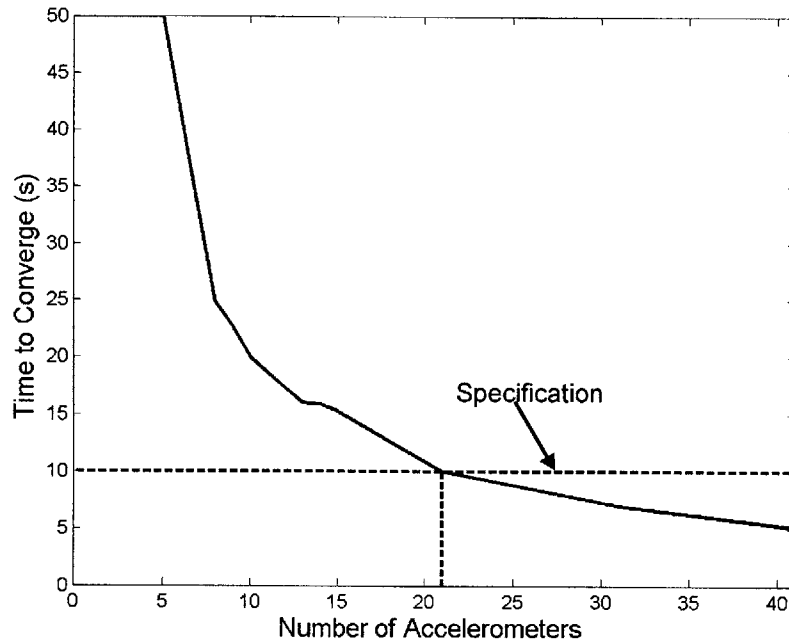
Figure 3.5. Convergence time for acceleration based estimates – Optimally placed accelerometers, 1-D large space structure, no rigid body motion.

Figure 3.6 shows the range sensor configurations (using both acceleration and vision measurements) that meet the desired specification. One configuration that meets the specification is a vision sample rate of 5 Hz and 8 optimally placed accelerometers. By using the two sensor types together, the requirements of a single system are reduced.
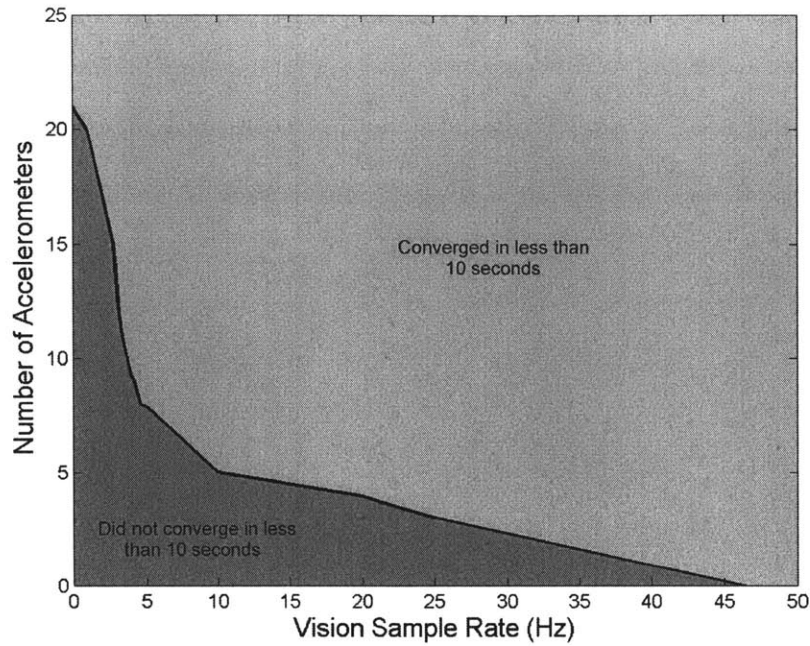
Figure 3.6. Sensor configurations for 1-D large space structure, no rigid body motion.

These simulations considered only vibrational motion. It should be noted that estimator based on only acceleration measurements is unable to approximate the rigid body motions. Vision measurements are required to estimate both the translational and rotational rigid body motions.

3.3 Planar Space Structure

3.3.1 Simulation Model

The estimation technique is not limited to simple beam structures. It is applicable to any flexible structure as long as there is some knowledge of the structures mode shapes, frequencies and dynamics. In this section, we apply this sensor fusion based estimation approach to the planar flexible structure shown in Figure 3.7.
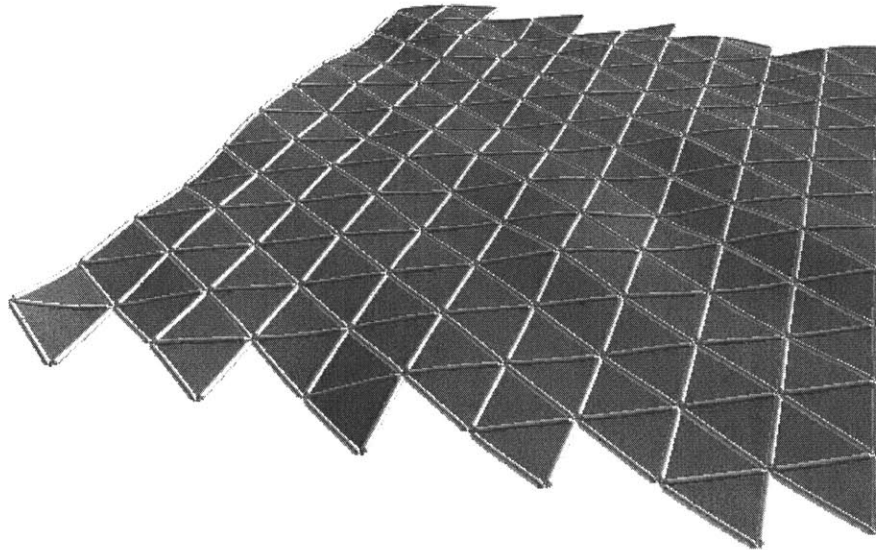
Figure 3.7. Three-dimensional structure used in simulation studies [21].

This flexible structure is representative of a space solar power station. The dimensions of the entire structure are approximately 2 km by 2 km. The dynamics of this structure are very slow, the period of the first mode is approximately 230 minutes. The mode shapes, frequencies and dynamics of this structure were provided by finite element analysis [28].

Simulated accelerometers are placed on the flexible structure using the D-Optimality criteria. These sensors are sampled at a rate of 100 Hz and measure the acceleration perpendicular to the surface of the structure. Gaussian sensor noise was added to the acceleration measurements with a standard deviation of 5% of the maximum acceleration. Range images were synthesized using an existing OpenGL code [21]. The vision sensor has an assumed resolution of 30 pixels by 30 pixels. The field of view and the location of the vision sensor were varied. Gaussian sensor noise was added to the range images with a standard deviation of 3% of the measurement in the range direction.

3.3.2 Estimator Performance

Simulations were performed while varying the vision sample rate and the number of structure-mounted accelerometers to evaluate the performance of this fusion-based approach. For these simulations, the modes were given random initial vibration amplitudes, each with the same expected energy. The total amplitude of the vibrations was approximately 25 m. The phase for each mode, φ_i, was randomly selected over the interval from 0 to 2π. Each configuration was tested using 10 different data sets to ensure independence on initial conditions. The remote-vision sensor is located above the center of the structure and has a field of view of 80 degrees by 80 degrees as shown in Figure 3.8.

The RMS shape error of the estimate is used to compare different sensor configurations. The dynamics of the structure are extremely slow, therefore a long amount of time will be required to accurately estimate the vibrations. Here, it is required that the shape estimate converges to within 0.25 m (1% of the initial deflection) RMS of the true value within 60 minutes (approximately ¼ of the period of the lowest mode).
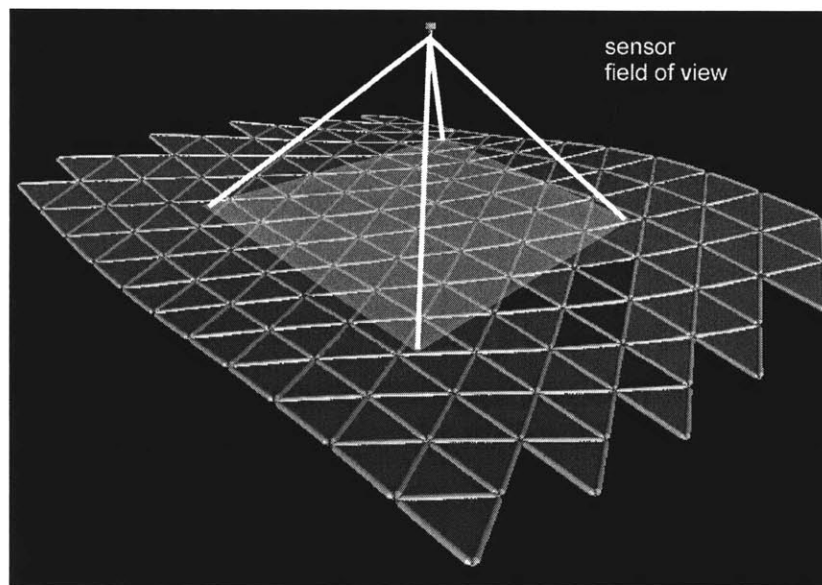
Figure 3.8. Camera placement for simulation studies [21].

Figure 3.9 shows the time required for a vision-based estimate to converge for various sample rates. The estimator is only able to meet the specification with a vision sample rate of 10 Hz or above. This sample rate is considerably lower than the rate required to for the 1-D space structure in Section 3.2.2 due to the slow system dynamics. However, this sample rate may still be unreasonably high for space-qualified hardware. This rate will be difficult to attain for a large area due to the operations the vision sensors perform. For example, a laser range finder requires nodding to scan a surface.
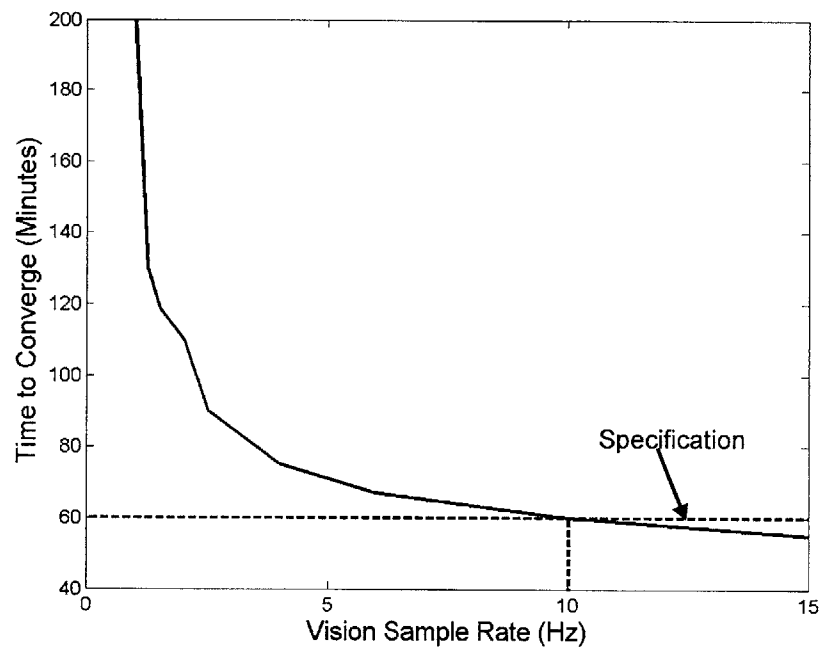
Figure 3.9. Convergence time of vision based estimates, planar large space structure.

Figure 3.10 shows the RMS shape error using a vision sample rate of 1 Hz, a reasonable speed for a space-qualified system. The estimate takes over 200 minutes to converge to within 25 cm RMS. This does not meet the specification.
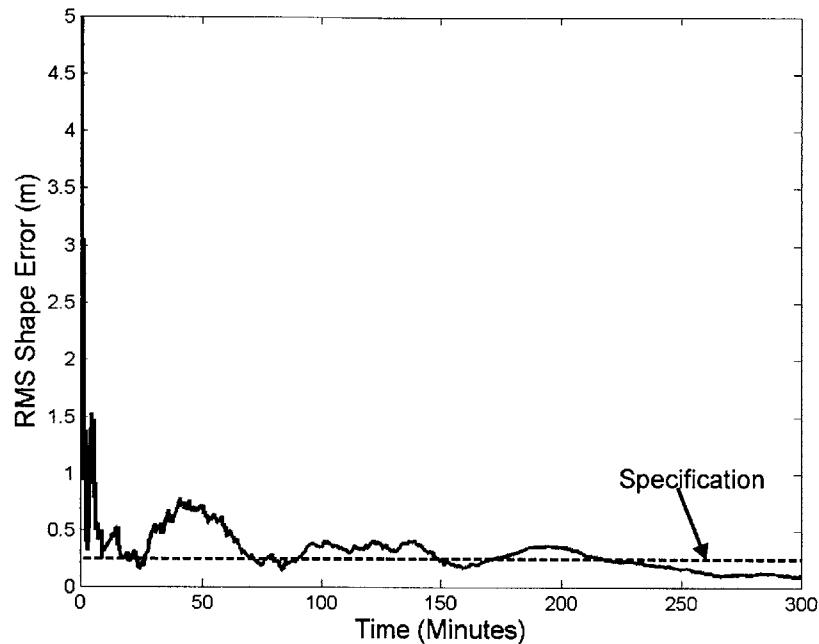
Figure 3.10. RMS shape error for a vision sample rate of 1 Hz.

Figure 3.11 shows the time required for the shape estimate to converge for different numbers of optimally placed accelerometers. The configurations that used less than 15 accelerometers did not converge within the total simulation time. For this planar large space structure, a total of 32 accelerometers are required to meet the specifications. The amount of infrastructure required makes this configuration undesirable. These simulations consider only vibrational motion. It should be noted that rigid body motions cannot be estimated using only accelerometers.

Figure 3.12 shows the RMS shape error for an estimate based on measurements from 10 accelerometers. The residual vibration for this configuration is still 5 m after 5 hours. This configuration does not meet the specifications.

Chapter 3. Simulation Studies   46
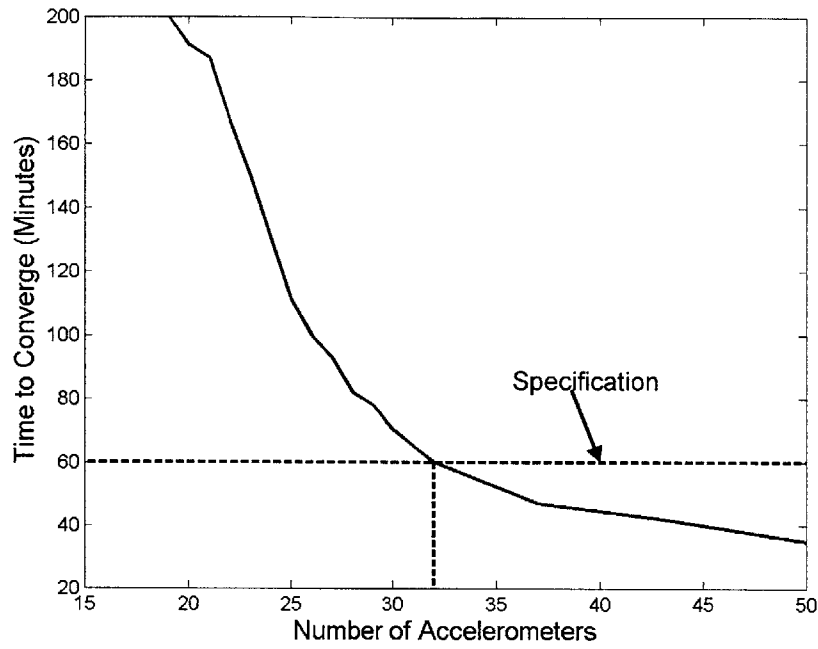
Figure 3.11. Convergence time for acceleration based estimates.
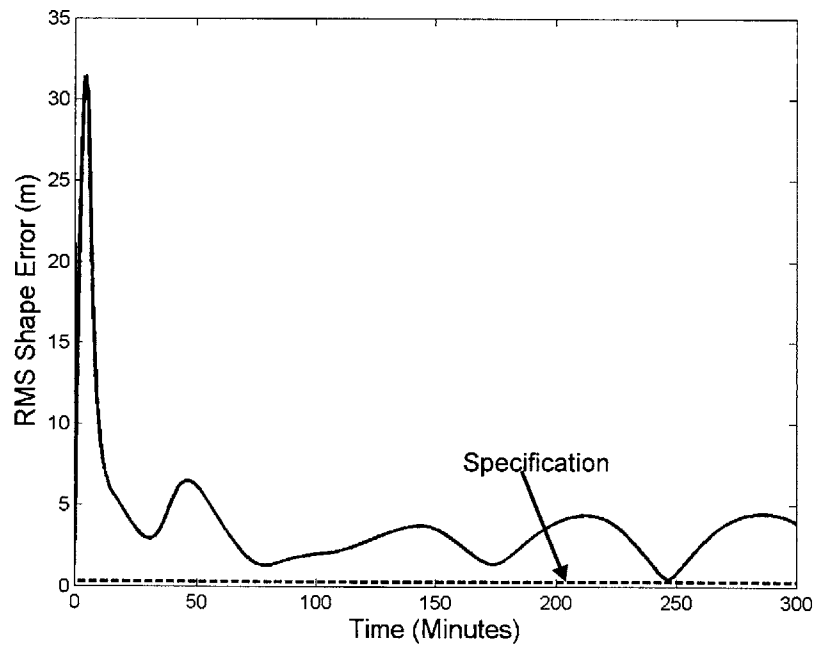
Figure 3.12. RMS shape error for an estimate using 10 accelerometers.

Chapter 3. Simulation Studies

Figure 3.13 shows the range of sensor configurations that meet the desired specification. One configuration that meets the specifications uses 10 accelerometers and a vision sample rate of 1 Hz. The convergence of the RMS shape error for this configuration can be seen in Figure 3.14. In this case, the shape error is able to converge in less than 60 minutes.
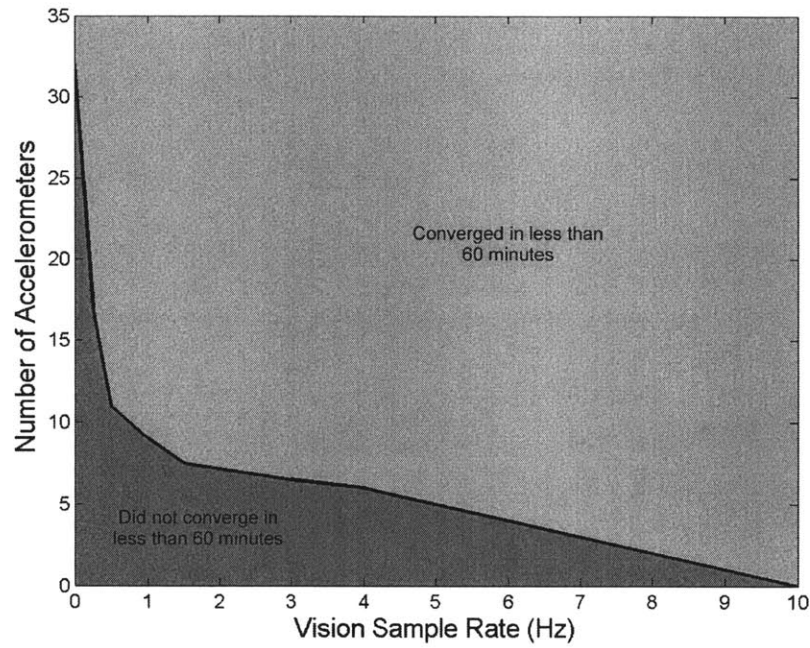
Figure 3.13. Sensor configurations for planar space structure.
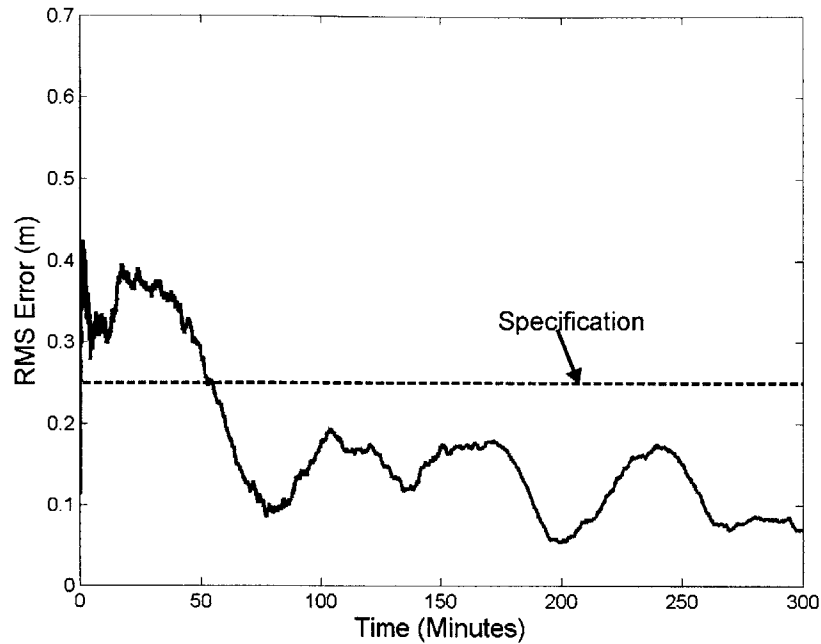
Figure 3.14. RMS shape error for estimated formed using 10 accelerometers and 1 Hz vision data.

3.3.3 Effect of Other Vision-System Parameters

Other parameters besides the vision sample rate can affect the performance of the estimator. In this section, the affect of vision sensor location and field of view are studied in simulation. For these simulations, the sensor is moved from the center of the structure to the side as shown in Figure 3.15. Initially, the field of view is 80 degrees by 80 degrees, identical to the case presented in Section 3.3.2. The performance specification chosen was identical to the specification in Section 3.3.2, the shape estimate must converge to within 0.25 m RMS of the true value within 60 minutes.
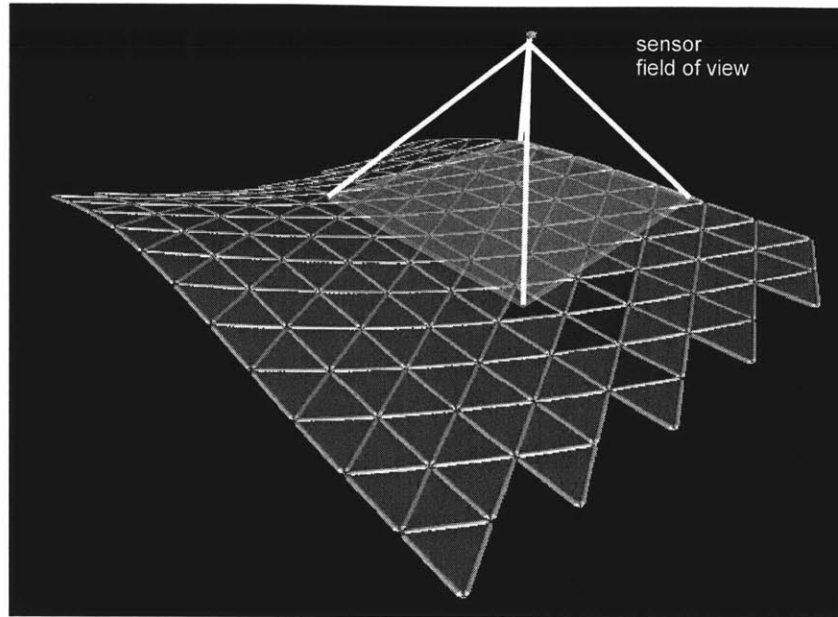
Figure 3.15. Sensor placement for simulation studies [21].

The performance of the estimator is expected to decrease due to this placement. This is due to the properties of the mode shapes of the structure that can be seen in Figure 3.16. Over the range viewed by the vision sensor, the first three mode shapes are easily distinguishable. However, the second and fourth mode shapes are very similar in the observable region. These modes are spatially aliased. As described in Section 1.2.2, the determinate of the modal correlation matrix can be used as an observability metric. In this case, the modal correlation matrix has large off-diagonal terms, and will have a smaller determinate. A summary of the determinate of the modal correlation matrices for different sensor configurations is shown in Table 3.2. Note that the determinate is smaller when the sensor is observing the side portion of the structure. Also note that the magnitude of the determinate decreases as the as the field of view is decreased.
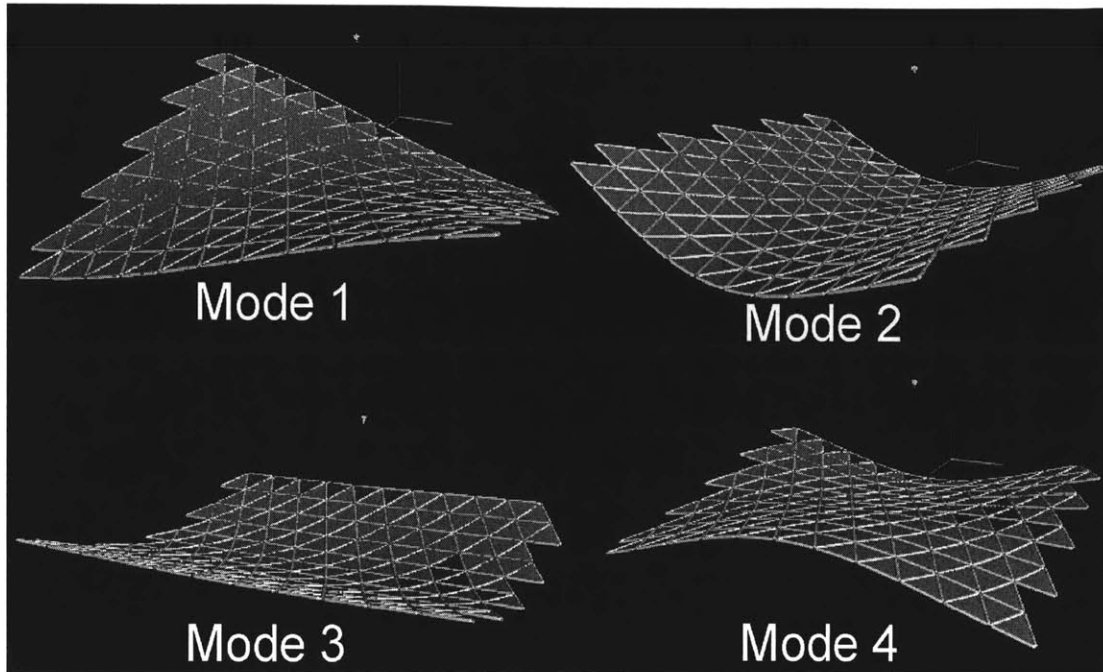
Figure 3.16. Mode shapes of 3-D large space structure [21].

Table 3.2. Observability metric for different vision sensor configurations

Vision Sensor Placement and Field of View	Determinate of Initial Modal Correlation Matrix
Center – 80 degrees x 80 degrees	2.7×10^{32}
Center – 65 degrees x 65 degrees	6.2×10^{30}
Center – 50 degrees x 50 degrees	4.7×10^{28}
Side – 80 degrees x 80 degrees	5.8×10^{31}
Side – 65 degrees x 65 degrees	7.7×10^{28}
Side – 50 degrees x 50 degrees	2.7×10^{27}

Figure 3.17 shows the sensor configurations that meet the desired specification when the vision sensor observes a side portion of the flexible structure. When comparing this plot with the case when the center of the structure was observed (Figure 3.13), the dividing line has shifted to the right. In the previous case, when the estimate was formed

using only vision data a sample rate of 10 Hz was required. In this case, a when only using vision data, a sample rate of 14.5 Hz is required. For this case, a reasonable configuration that meets the specification would be a vision sample rate of 2 Hz and 10 on-board accelerometers.

Figure 3.17. Sensor configurations for planar large space structure, second viewpoint, field of view 80 degrees by 80 degrees.

As was shown in Table 3.2, if you decrease the size of the viewing area, the observability metric also decreases. This effect was tested in simulation. With the sensor located above the side of the structure, as shown in Figure 3.15, the field of view was reduced to 65 degrees by 65 degrees. Figure 3.18 shows the sensor configurations that meet the specification for the 65 degrees by 65 degrees field of view. In this case, the dividing line is moved even further to the right. When using only the vision data, a sample rate of 18.5 Hz is required to meet the specifications. This rate will be

unreasonably high for a space-qualified vision system. If the accelerometers and vision system are used together, the specification can be met with a reasonable vision sample rate of 4 Hz and 10 structure-mounted accelerometers.

Figure 3.18. Sensor configurations for a planar large space structure, second viewpoint, field of view 65 degrees by 65 degrees.

If we decrease the size of the field of view of the vision sensor even more, the estimator performance will continue to decline. This can be predicted by the magnitude of the determinate of modal correlation matrix. Figure 3.19 shows the sensor configurations that meet the specification when the field of view of the vision system is reduced to 50 degrees by 50 degrees. The dividing line has moved even further to the right. In this case, when using only vision data a sample rate of 31 Hz is required to meet the specifications. If the accelerometers and vision system are used together, the specification can be met with a reasonable vision sample rate of 5 Hz and 14 structure-

mounted accelerometers, higher than the vision sample rate of 1 Hz and 10 structure-mounted accelerometers required when using a field of view of 80 degrees by 80 degrees.

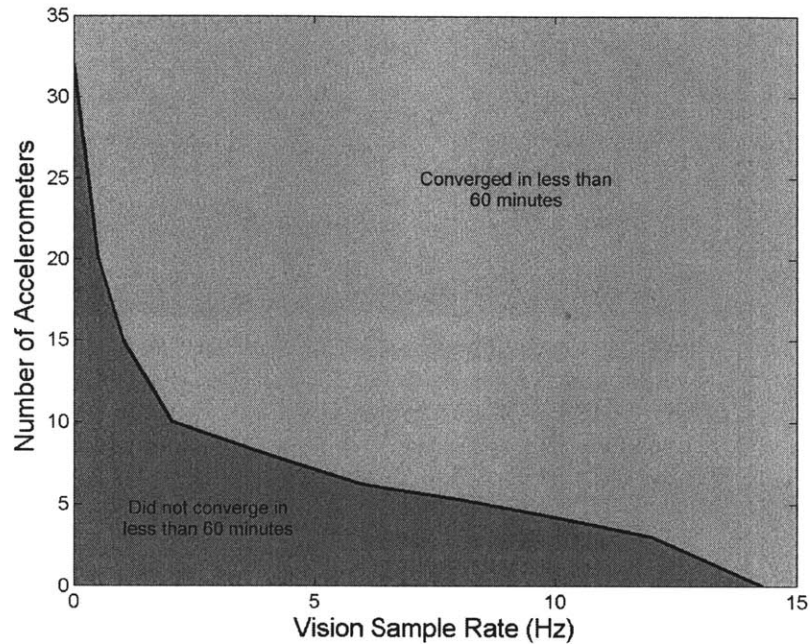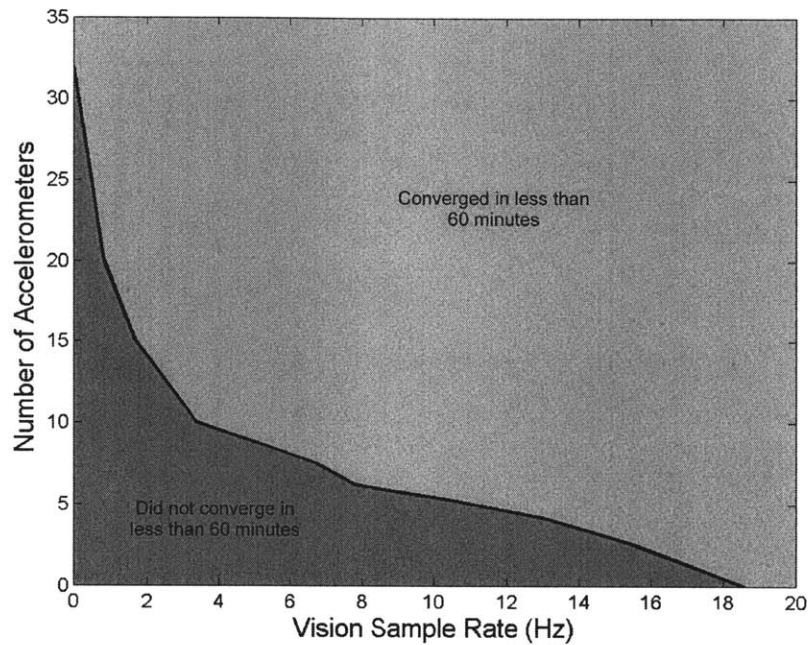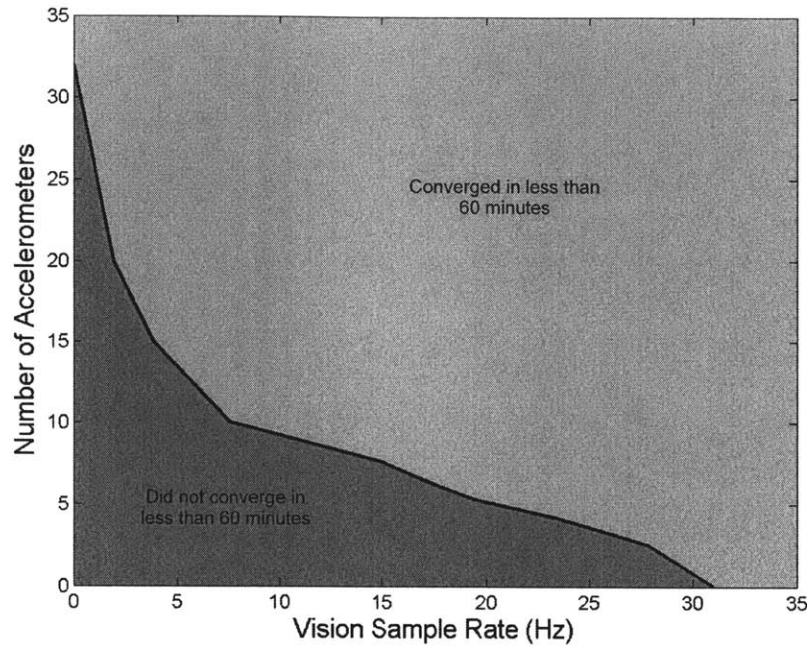*Figure 3.19. Sensor configurations for 3-D large space structure, second viewpoint, field of view 50 degrees by 50 degrees.*

It is important to note that the vision sensor does not need to observe entire structure to achieve an accurate estimate of the vibrations. The results presented above show that the performance of the estimator degrades gracefully as the scanned area decreases.

3.4 Implementation in the Feedback Loop

3.4.1 Problem Definition

The output of the estimator is the magnitude of the modal coefficients, their derivatives, the modal frequencies and the modal damping. These values can be used by control robots during the construction of the large space structure. It is important that vibrations be controlled during the structure's transportation and assembly in order to prevent damage to both the structure and the robots.

This section evaluates the performance of a cooperative control approach for the transportation of large flexible space structures developed in [13] for various sensor configurations. This approach is depicted in Figure 3.20. This figure shows a large flexible space structure being transported by two robots equipped with thrusters and manipulators. Estimates of the modal coefficients are provided to the transportation robots by fusing information from structure-mounted accelerometers and remote-vision sensors on global-observer robots.
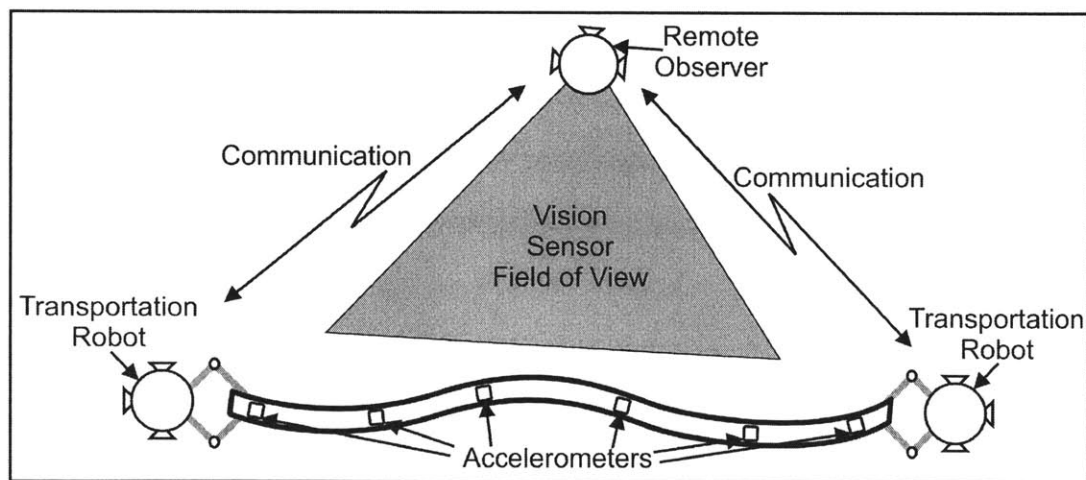
Figure 3.20. Maneuvering of large flexible structure by cooperative robots [13].

This is just one of a number of robot controllers used to control the vibrations of flexible structures [5, 16, 23]. All such controllers require some knowledge of the structures vibration. This estimation algorithm could also be used in terrestrial applications such as cranes or other construction equipment [5].

3.4.2 Control Architecture

The control architecture decouples the rigid-body motion from the structural vibration. This decoupled controller consists of two loops. The inner loop is an active modal damping controller that uses the robot manipulators to damp out any structure vibration. The outer loop is a rigid body motion controller that controls the position and orientation of the robot structure system using the robots' thrusters. The inner loop of the control algorithm, shown in Figure 3.21, controls the y-component of the robot structure interaction forces. The interaction forces are given by:

$$\mathbf{F} = \mathbf{K}_r \left(\mathbf{r} - \mathbf{r}_{ref} \right) + \mathbf{B}_r \left(\dot{\mathbf{r}} - \dot{\mathbf{r}}_{ref} \right) + \mathbf{K}_q \mathbf{q} + \mathbf{B}_q \dot{\mathbf{q}}$$

where $\mathbf{r}$ is the position of the robot's center of mass and $\mathbf{q}$ is the vector of the structure's vibrational modal coefficients. The gains $\mathbf{K}_r$ and $\mathbf{B}_r$ can be thought of as the stiffness and damping of a virtual spring and dashpot between the robots and the structure, while $\mathbf{K}_q$ and $\mathbf{B}_q$ are the feedback gains of the modal damping terms that control the structures vibration. Details of the gains selection can be found in [13].
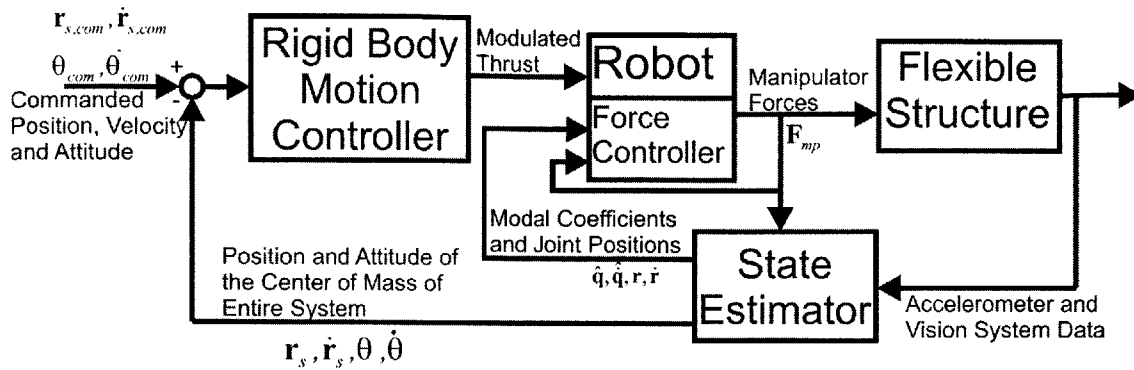
Figure 3.21. Control architecture [13].

The objective is to transport the structure to rest at its pre-assembly position while minimizing fuel usage and structure vibrations. The solution to the minimum fuel problem is a bang-bang control. However, these control inputs would excite vibration in the structure. Therefore, the manipulators damp out the vibration to prevent damage to the module and robots.

The performance of the decoupled controller with different sensor architectures was studied in simulation. Figure 3.22 shows the simulated slew maneuver, in which two 100 kg robots grasp either end of a 200 m long flexible structure. The robots transport the center of the beam 150 m in the X and Y direction while rotating the structure by 90 degrees.
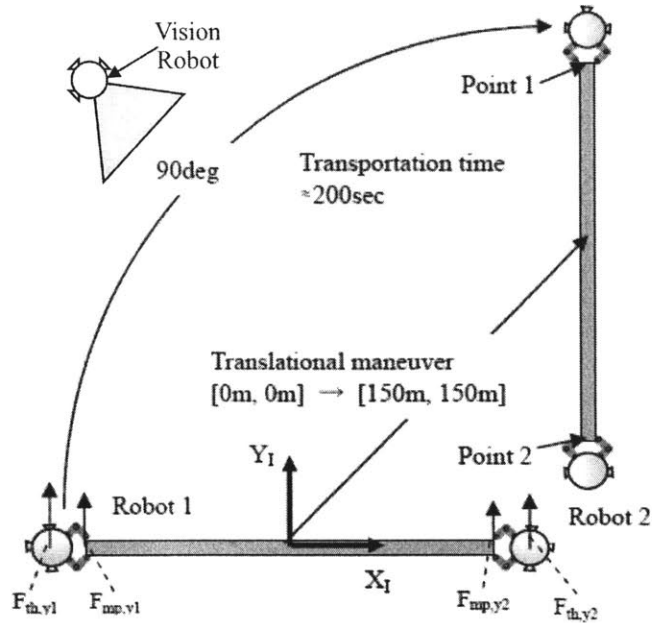
Figure 3.22. Transportation manuever using a team of robots [13].

The sensor configuration tests varied two parameters: the number of accelerometers on the flexible structure, and the sample rate of the vision sensor. It is assumed for all simulations that there is a single vision sensor observing the structure with a sensor noise of 0.5 m, a reasonable value based on sensors proposed for space applications [43]. The vision sensor rotates to maintain a clear view of the entire structure during the manuever. It is also assumed that the accelerometers are sampled at a rate of 100 Hz and have a sensor noise of 0.1 m/s^2. The locations of the accelerometers were chosen using the D-Optimality Criteria that maximizes the observability of the modes [38], the same technique used in Section 3.2.2. It is also assumed that the force sensors are sampled at a rate of 100 Hz and have a sensor noise of 1 N. Details of the simulation parameters can be found in Table 3.3.

Table 3.3. Transportation simulation parameters.

Parameters	Values
Flexible Structure	Mass m_b :600kg, Length L : 200m, Inertia I_{zz} : 2×10^6 kgm^2 Natural Frequencies: 0.20, 0.55, 1.08, 1.78, 2.67, 3.75, 5.02Hz (seven modes considered)
Robot	Mass m_r:100kg
Thrusters	Thrust F_{max} : ±20N or 0 N (X_G, Y_G direction) Minimum ON/OFF time : 50msec Response Delay: 50msec
Manipulators	Length:1m + 1m (2-DOF)
Accelerometers	Sample Rate:100 Hz Sensor Noise: σ_a=0.1 m/s^2
Vision Sensors	Sensor Noise: σ_v=0.5 m
Force Sensors	Sensor Noise: σ_F=1N
Specifications	Residual Vibration < 5cm peak-to-peak

Small errors in the estimates of the modal coefficients result in residual vibration in the structure. Therefore, the magnitude of the residual vibration can be used to compare the estimator performance for different sensor configurations. It is important that the residual vibration at the beam-ends at the conclusion of the transportation be small so that the subsequent assembly tasks can be executed properly. Here it is assumed a residual vibration of less than 5 cm, peak-to-peak, is required. This specification was chosen based on the projected size of robot grippers [9].

3.4.3 Results

Figure 3.23 shows the magnitude of residual vibration present when only the vision sensor is used for various sample rates. The estimator is only able to meet the specifications when the vision sample rate is above 21 Hz, a sample rate that may be unreasonably high for space-qualified hardware.
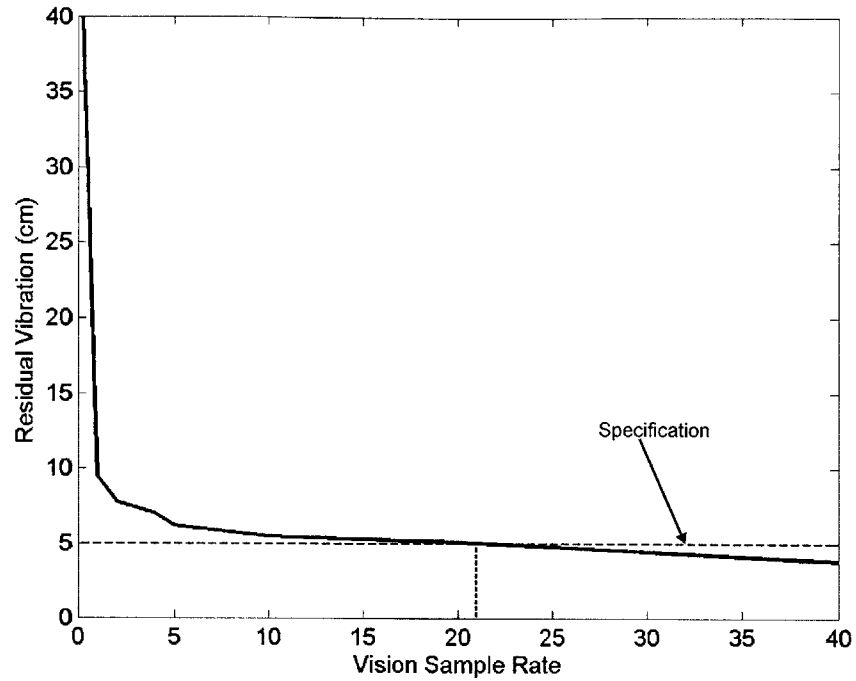
Figure 3.23. Residual vibration of vision based estimates.

Figure 3.24 shows the end deflection of the flexible structure during the maneuver when using an estimate obtained from 2 Hz vision data, a reasonable rate for a space-qualified vision system [43]. Following the maneuver, the structure continues to vibrate with a peak-to-peak magnitude of 8 cm. This configuration does not meet the specifications.
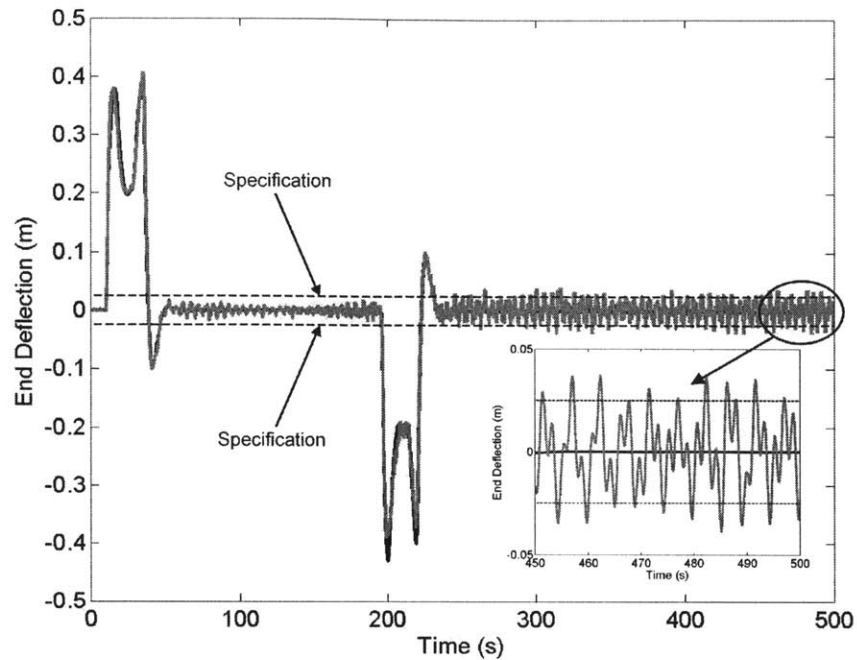
Figure 3.24. End deflection of beam during maneuver using estimate obtained from 2 Hz vision sensor.

Figure 3.25 shows the magnitude of the residual vibration versus the number of accelerometers on the structure when only accelerometers are used. Even for this simple one-dimensional beam structure, 15 accelerometers are required to meet the specification when accelerometers are used alone. For a planar or 3-dimensional structure this number would be many times higher. A large number of accelerometers may be undesirable due to the amount of infrastructure required for each sensor.

Figure 3.26 shows the end deflection during a maneuver when using an estimate based on measurements from 7 accelerometers. The structure has residual vibration of a magnitude of 10 cm peak-to-peak. This configuration does not meet the desired specification.
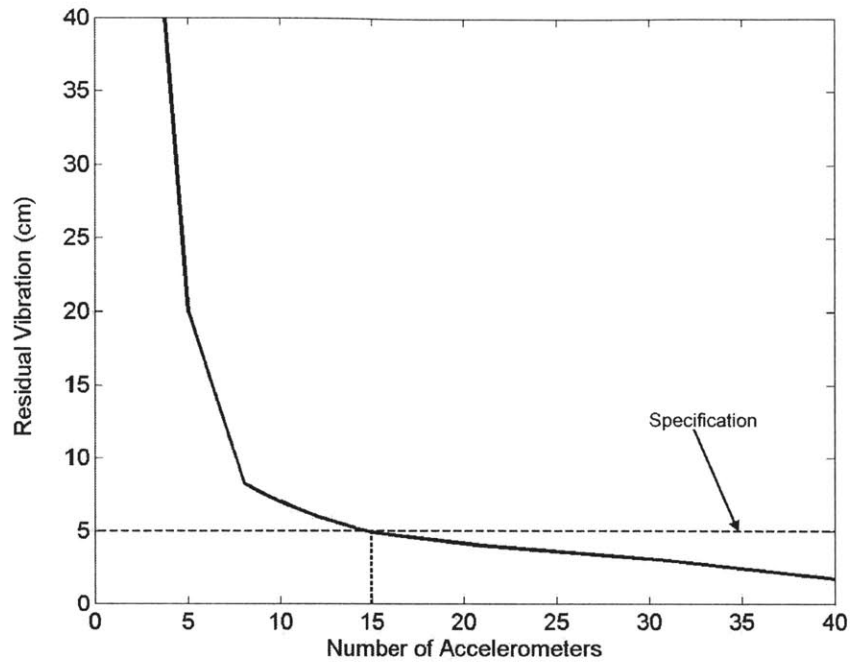
Figure 3.25. Residual vibration of acceleration based estimates.
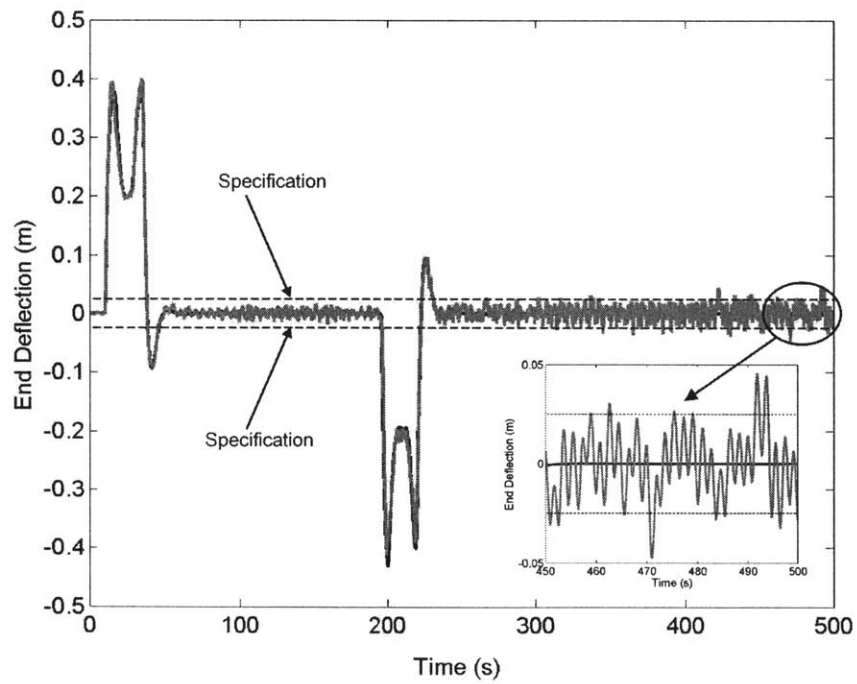
Figure 3.26. End deflection of beam during maneuver using estimate obtained from 7 accelerometers.

Figure 3.27 shows a range of sensor configurations that meet the specification. One configuration that meets the specifications uses 7 accelerometers and a vision sample rate of 2 Hz. The end deflection during the maneuver for this configuration can be seen in Figure 3.28. The peak-to-peak residual vibration for this configuration is 2.5 cm, well below the specified value of 5 cm.
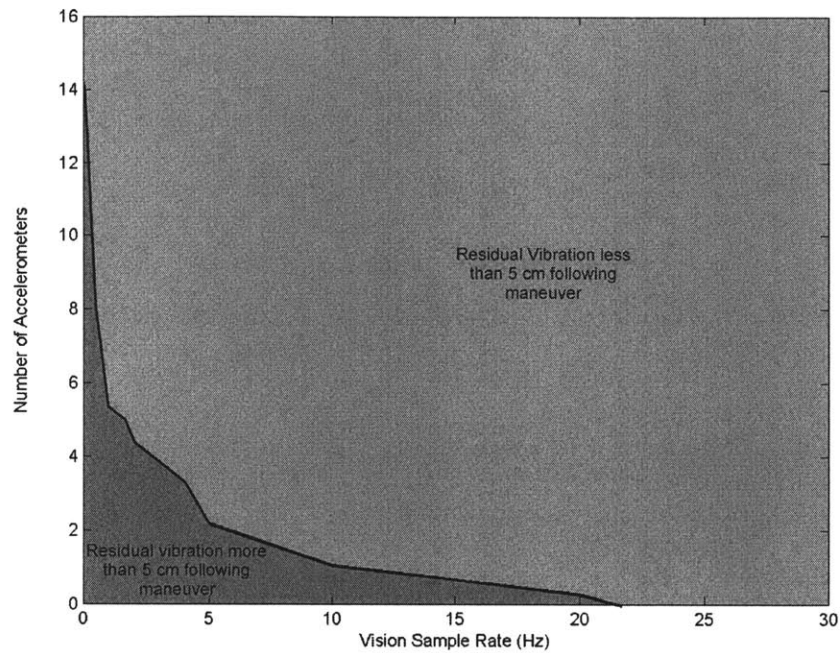
Figure 3.27. Sensor configurations for the estimator in the feedback loop of the LSS transportation controller.
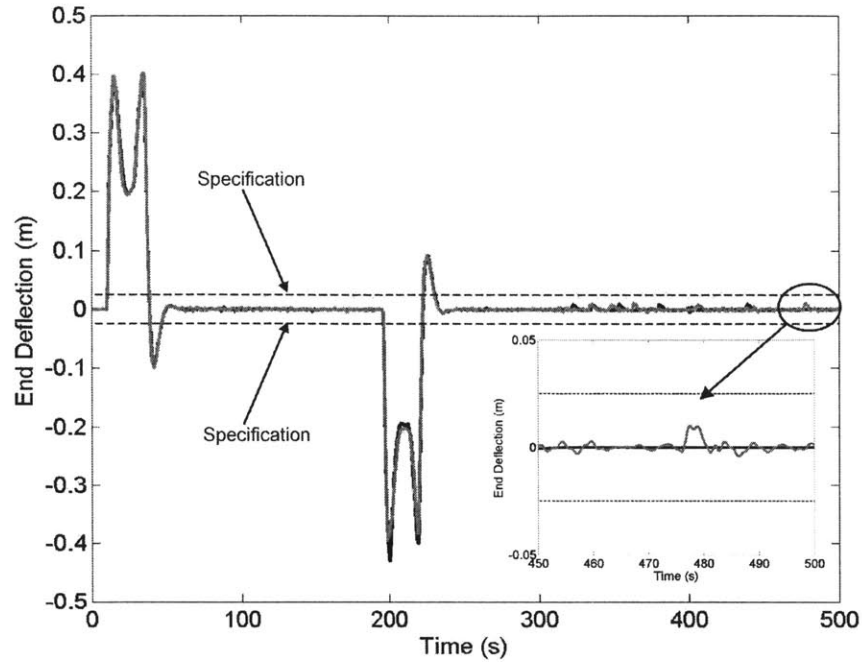
Figure 3.28. End deflection of beam during maneuver using estimate obtained using 7 accelerometers and 2 Hz vision data.

3.5 Summary

This chapter presented the performance of the estimator for three different simulated cases: a freely vibrating one-dimensional space structure, a freely vibrating planar space structure, and in the feedback loop for a large space structure transportation controller. In all three cases it was found that the estimator using the data from both the structure-mounted accelerometers and remote-vision sensors had higher performance than the estimators using only a single type of sensor.

CHAPTER

4

EXPERIMENTAL VERIFICATION

4.1 Experimental Platform

A series of experimental studies were conducted in the laboratory to determine if any unmodeled effects degrade the performance of the estimator. These studies used the Robotic Team Interactive Microgravity System (ROTIMS) in the MIT Field and Space Robotics Laboratory. For these experiments, the system was configured with a granite surface plate, two floating modules, and a flexible structure.

The granite surface plate serves as the base for the experimental system. The surface plate is 2.2 meters long by 1.3 meters wide and is finely leveled to simulate a two-dimensional microgravity environment. The floating modules were designed to operate on top of the micro-polished granite surface. These modules are supported by three low-friction, flat floatation bearings. The floatation bearings run on compressed carbon dioxide, which is stored on-board the modules. For this series of experiments, a flexible panel was mounted between two floating modules to simulate a one-dimensional space structure. Details of the structure are presented in Section 4.2. The full experimental setup is shown in Figure 4.1.
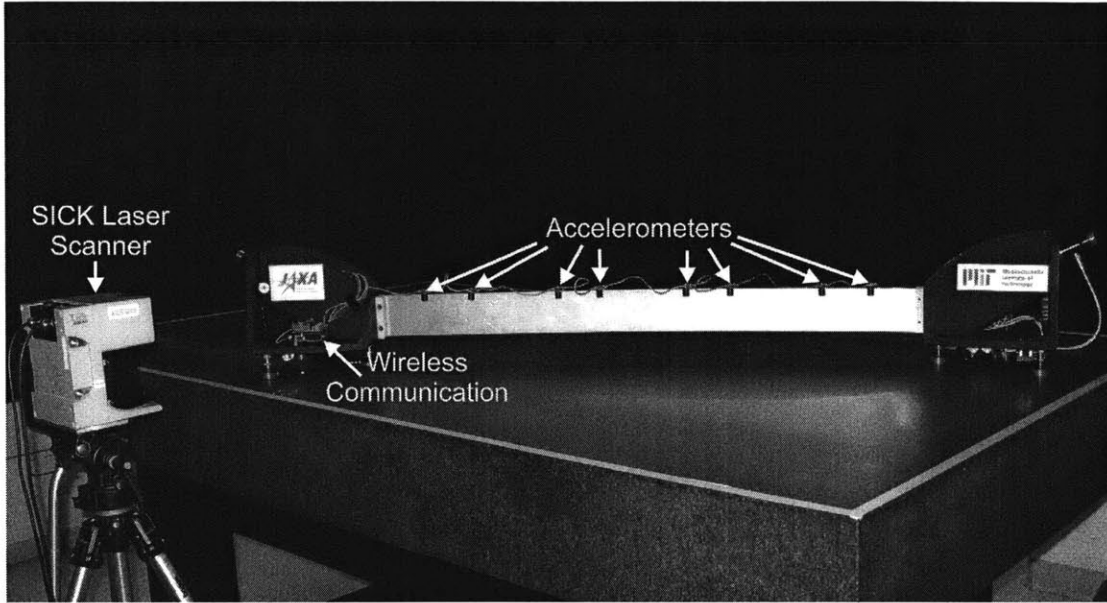
Figure 4.1. Experimental setup.

The flexible structure is equipped with eight accelerometers manufactured by Analog Devices. The accelerometers were placed using the D-Optimality criteria [38] as shown in Figure 4.2. These accelerometers have a measurement range of +/- 1.2g and a measurement variance (σ_a^2) of $0.013g^2$. The accelerometers are sampled at a rate of 267 Hz by a PIC microcontroller system designed by Dr. Matthew Lichter. These values are then transmitted wirelessly to a ground computer system and are logged for post-processing.
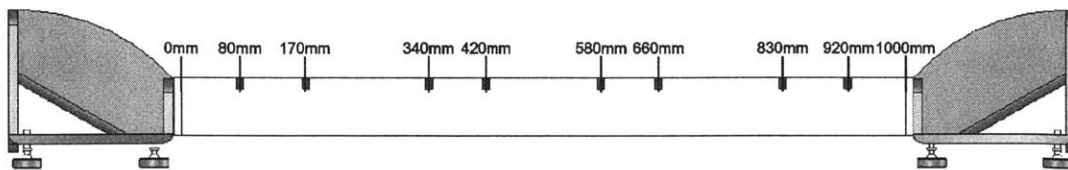
Figure 4.2. Accelerometer placement for experimental studies.

A SICK LMS 291 [33] laser scanner is mounted on a tripod next to the air table to provide the vision deflection measurements of the flexible structure. The details of the structure are presented in Section 4.2. All of the range data was collected and logged using software developed by Marcos Berrios. This system is able to capture 77 sweeps per second at an angular resolution of 1 degree. Like any other laser measurement system, the measurements are noisy, and regions of the measured structure may be missing due to limited reflectivity. The measurement variance in the range direction (σ_v^2) for this system was calculated in to be 1.7mm^2.

Figure 4.3 shows a representative data sweep generated by this system. The SICK is unable to detect the floating modules due to their surface properties. Therefore, there are large steps at the edge of the flexible structure. The useful data is extracted by identifying these large steps.
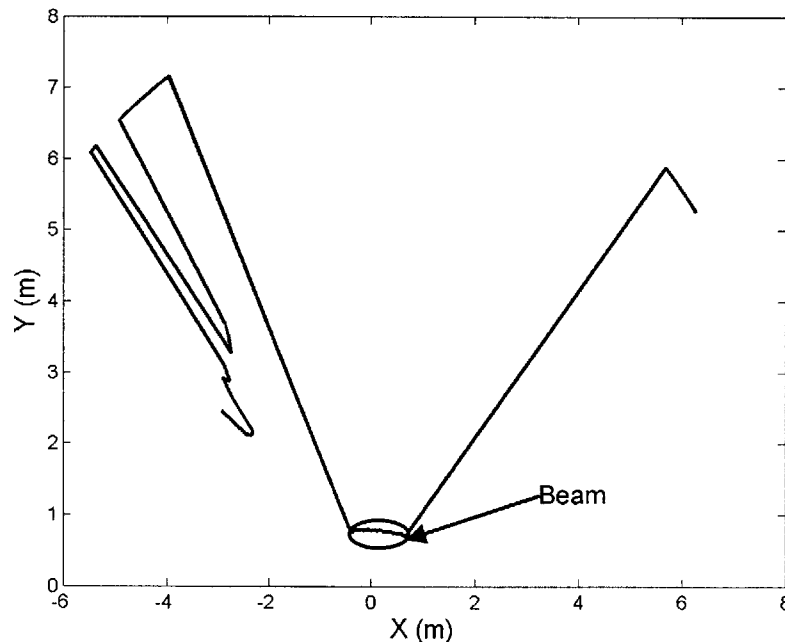
Figure 4.3. Sample data from a single sweep of the SICK laser scanner.

A camera, made by Videre Design, mounted above the air table observed the structure to provide a ground-truth. This overhead camera collected images at a rate of 15 Hz. Software, written by Dr. Yoji Kuroda, processed the images in real-time in order to track seven points on the vibrating structure. These measurements have a resolution of 6mm.

4.2 Structural Model

A simple beam structure was designed for the experiments. This structure is a thin beam made of stainless steel, which is clamped at each end to a floating module (see Figure 4.2). The mode shapes and frequencies were computed using the FEM software ADINA. A summary of these properties can be found in Table 4.1.

Table 4.1. Properties of experimental structure.

Parameters	Values
Material	Stainless Steel
Dimensions	Flexible Beam - 1000mm long, 80mm tall, 0.76mm wide
Stiffness	0.190 GPa
Mass	6.5 Kg Tanks Full, 5.6 Kg Tanks Empty
Frequencies	0.82Hz, 2.07Hz, 5.03Hz, 9.59Hz

An interesting property of this experimental setup is that the mass of the structure will vary during the course of an experiment due to the carbon dioxide used by the floatation bearings. This will cause the mode shapes to slightly change and the frequencies to increase. This effect is negligible over the course of a single trial (over 45 seconds less than 20 grams of carbon dioxide is used). However, the difference between trials completed when the tanks are full would be substantially different than when the tanks are nearly empty. Rather than change the a priori knowledge of these values in the

estimator, the same values are used for each trial. This approach tests the robustness of the estimation algorithm to real world effects.

Structural vibrations are induced by hand. The structure is deformed and then carefully released in order to minimize any translation or rotational motion. It is necessary to reduce these motions to ensure the structure will remain vibrating on the table long enough to allow the estimator to converge. Once the structure has been released the data collection begins. All of the measurements are time-stamped to ensure the different measurements will be coordinated.

4.3 Results

The experimental data was analyzed offline. This analysis varied two parameters: the number of accelerometers used in the estimation and the sample rate of the vision sensor. The number of accelerometers and the vision sample rate were varied by ignoring the appropriate measurements.

The RMS error in the shape estimate at the 7 points tracked by the overhead camera is used to compare the different sensor configurations. The shape estimate neglects rigid body motion. Here, the comparison metric is the time required for the RMS error to converge within 2.4 cm (4 pixels of the overhead system) of the ground truth. This must happen within 10 seconds.

Ten different sets of experimental data were analyzed. The first vibrational mode was dominant in 5 of the data sets, and the second vibrational mode was dominant in the other 5 data sets. A total of 4 modes were estimated.

Figure 4.4 shows how the convergence rate varies for estimates using only measurements from the SICK laser scanner. Estimates using vision data at a sample rate below 4.5 Hz are unable to converge within the timeframe of the experiment. The

estimate is only able to meet the desired specification when the sample rate is 28 Hz or higher. This sample rate is unreasonably high for real-time implementation of the estimator.
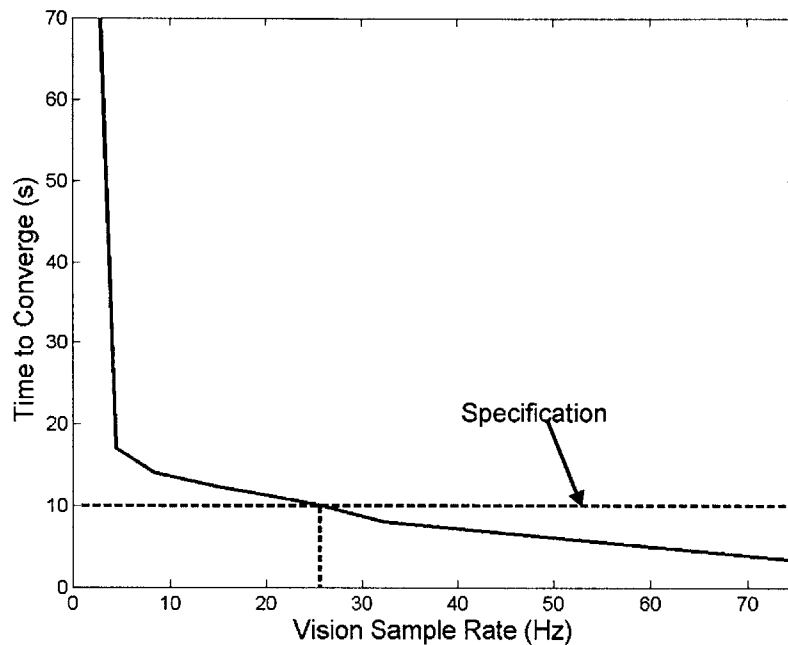
Figure 4.4. Convergence of vision based estimates.

Figure 4.5 shows the shape estimate at a point on the structure using 9 Hz vision data. Nine Hz is a reasonable rate for the online implementation of this system. The estimator does good job at estimating the phase of the vibration, but it is unable to converge to the correct amplitude within the specified time. Figure 4.6 shows the RMS error for this configuration. The estimate is unable to converge to within the desired tolerance within 10 seconds.

Figure 4.5. Deflection of a point 8 cm along the structure using a estimate from 9-Hz vision data
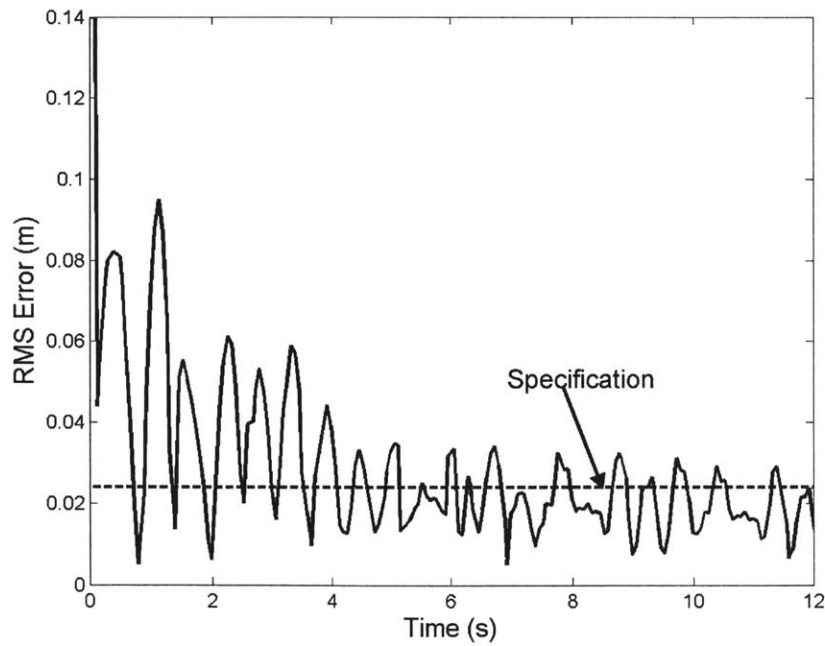
Figure 4.6. RMS error of an estimate using 9-Hz vision data.

Figure 4.7 shows how the convergence rate varies for estimates using only measurements from the accelerometers. Estimates formed using 1 accelerometer are unable to converge during the length of an experimental trial. The estimate is only able to meet the desired specification when 6 or more accelerometers are used. This is an unreasonable number for such a simple structure. For a larger, more complex structure many more accelerometers would be required. It should also be noted that rigid body motions cannot be estimated with only accelerometers.
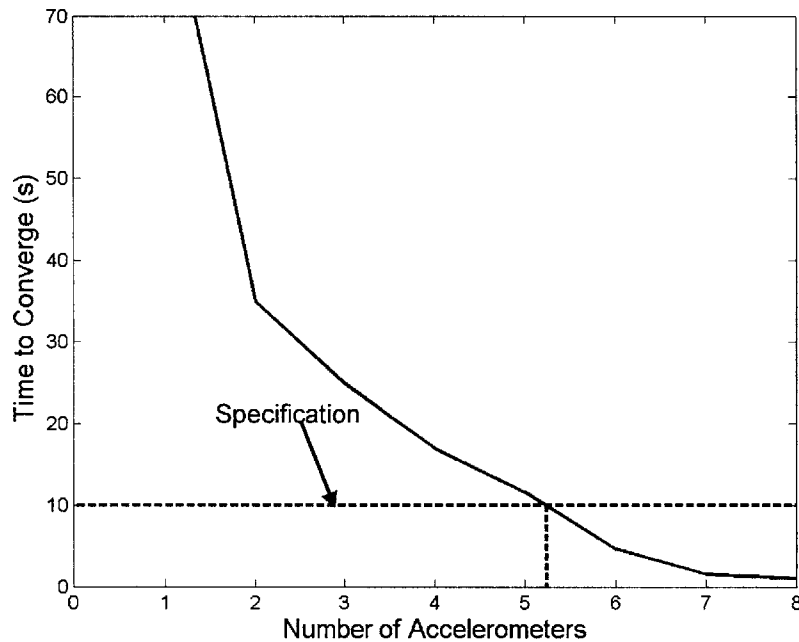
Figure 4.7. Convergence of acceleration-based estimates.

Figure 4.8 shows the shape estimate at a point on the structure using data from 3 accelerometers. Three accelerometers are a reasonable number for a structure of this size. The estimator converges to the proper phase but is unable to reach the appropriate amplitude in the specified amount of time. Figure 4.9 shows the RMS error for this configuration. The estimate is unable to converge within 10 seconds.
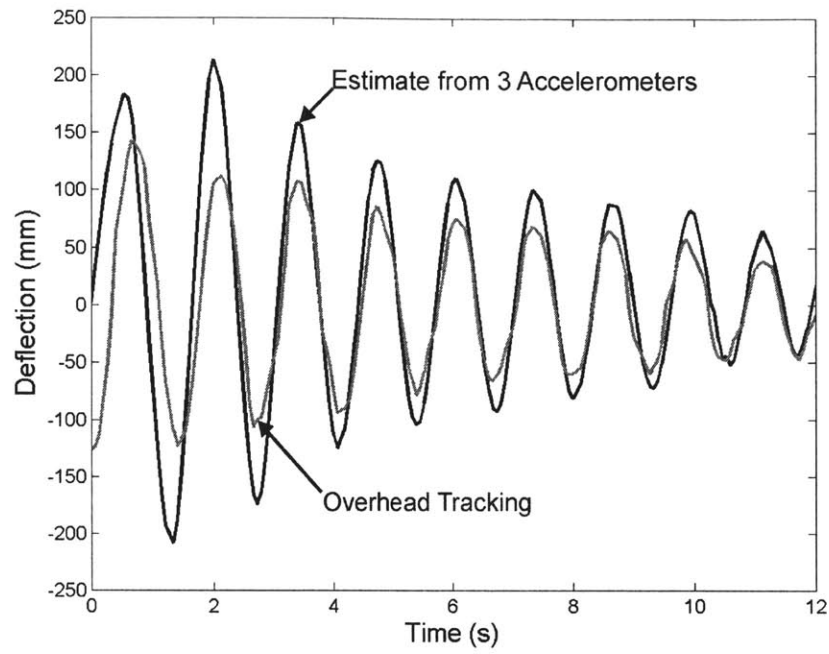
Figure 4.8. Tracking of a point 8 cm along the structure using an estimate from 3 accelerometers.
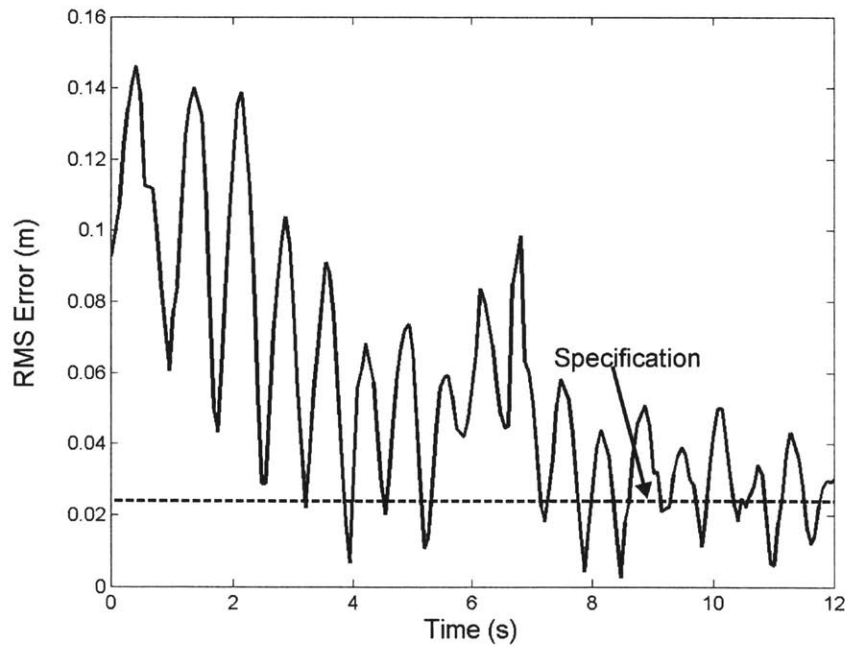
Figure 4.9. RMS error of an estimate using 3 accelerometers.

Figure 4.10 shows a range of sensor configurations that meet the specification. One configuration that meets the specifications uses 3 accelerometers and a vision sample rate of 9 Hz. This is a reasonable configuration for real-time implementation of this system.
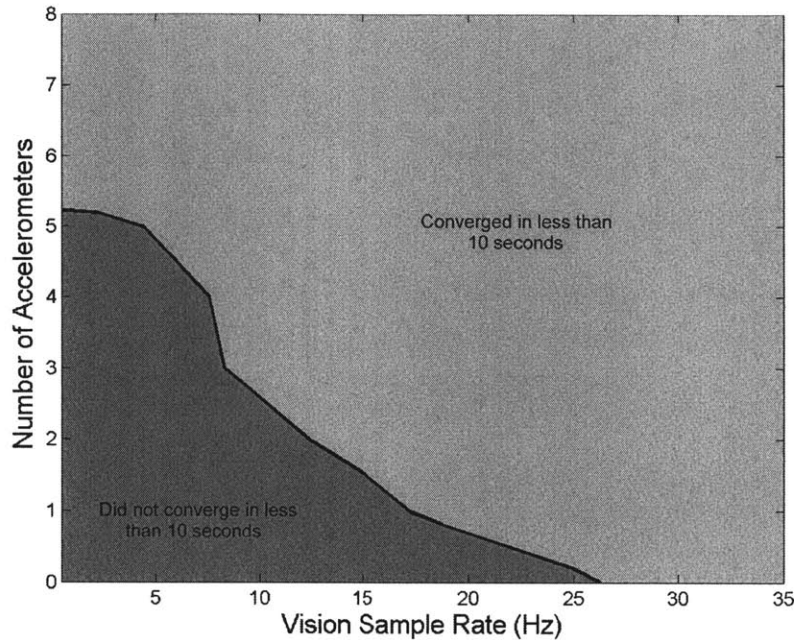
Figure 4.10. Sensor configurations, experimental results.

Figure 4.11 shows the shape estimate at a point on the structure using data from 3 accelerometers and 9 Hz vision data. After 5 seconds, the deflection measured by the overhead camera and the estimated deflection are nearly identical. Figure 4.12 shows the RMS error for this configuration. The estimate is able to converge to within the desired tolerance within 7.5 seconds. This configuration meets the specifications.
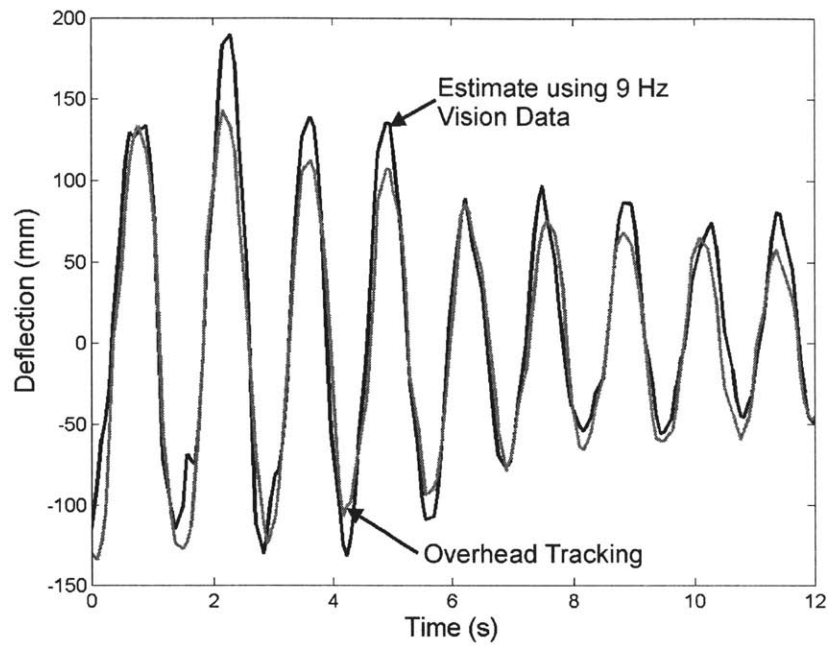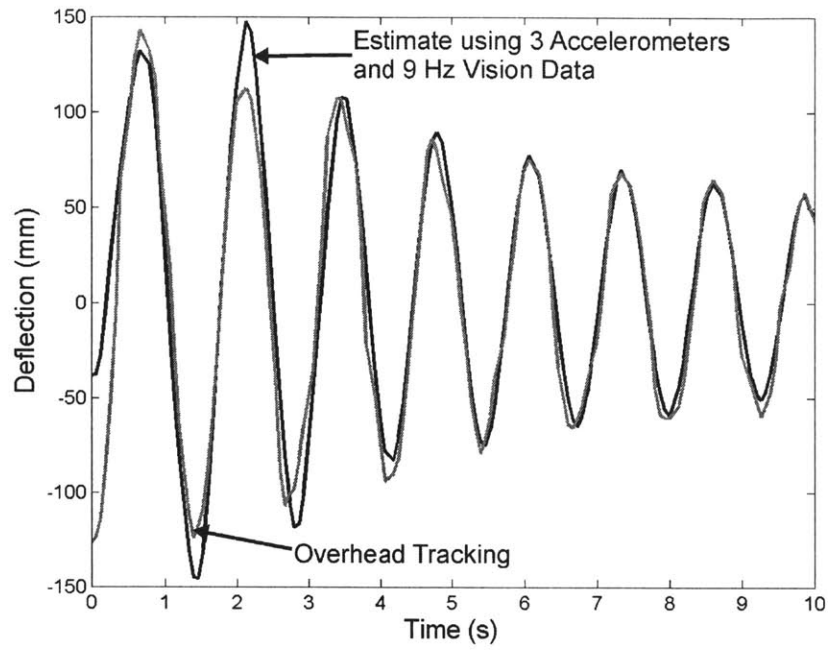
Figure 4.11. Tracking of a point 8 cm along the structure using an estimate from 3 accelerometers and 9 Hz vision data.
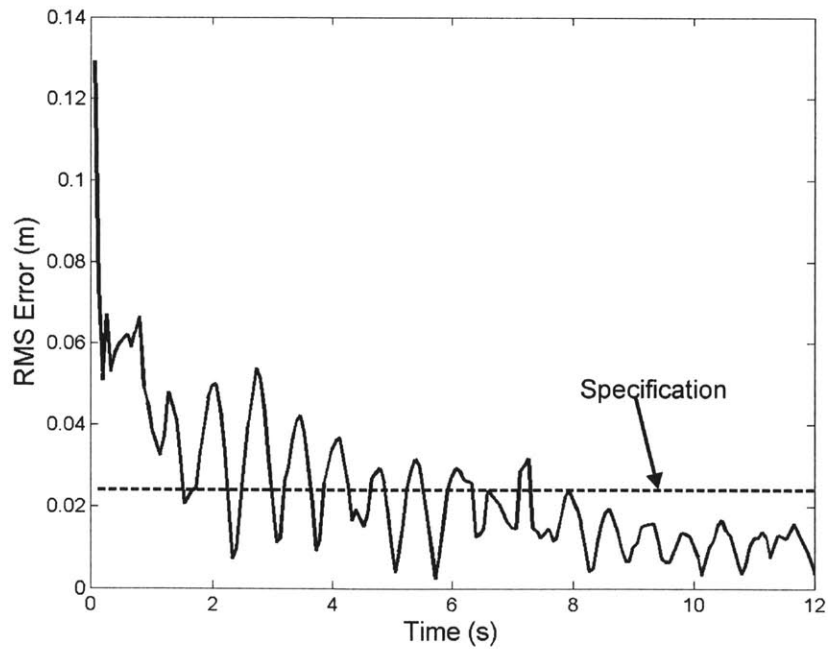
Figure 4.12. RMS error of an estimate using 3 accelerometers and 9 Hz vision data.

4.4 Summary

This chapter presented experimental validation of the fused estimation approach. These results corroborated the results from the simulation studies. It was found that when only using a single type of measurement, 6 accelerometers or a vision sample rate of 27 Hz is required to achieve an accurate estimate of the shape of the flexible structure. However, if the two sensor types are used together, an accurate estimate could be achieved with a limited vision sample rate of 9 Hz and three structure-mounted accelerometers.

5

SUMMARY & CONCLUSIONS

5.1 Conclusions

This thesis developed an architecture using remote-vision sensors and structure-mounted accelerometers together in concert to estimate the shape and dynamic parameters of a vibrating large space structure. This architecture was analyzed for various sensor configurations to determine the effectiveness of this approach. It was found both in simulation and experimentally that by using a combination of these sensors an accurate estimate can be achieved while easing the requirements of the individual sensor systems.

Chapter 1 provided motivation for this work and presented relevant background literature. Future space structures such as space solar power plants are expected to be large and complex. Robotic systems will be necessary for the on-orbit construction of these large space structures. Robots will require knowledge of the structure's vibrations in order to efficiently manipulate these flexible structures. Both remote vision sensors and structure-mounted sensors have been used to estimate the dynamics and shape of flexible large space structures, but no one has considered the benefits of combining measurements from these two types of sensors.

Chapter 2 presented the architecture for estimating the shape and dynamic parameters of a vibrating large space structure using remote vision sensors and structure-

mounted accelerometers. In the first step, the vision data goes through a modal decomposition. In the second step, a multi-rate Kalman filter fuses the coarse estimates of the modal coefficients from the vision system with the measurements from the accelerometers. The Kalman filter produces estimates of the modal frequencies, modal damping, modal coefficients, and their derivatives. In the final step, the modal coefficients are recombined with the mode shapes to produce an estimate of the shape of the structure.

Chapter 3 presented simulation results evaluating the fused estimation approach. Simulations were conducted for three different cases: a one-dimensional space structure, a planar space structure, and a space structure being manipulated by free-flying robots. In all three cases it was found that an accurate estimate of the shape of flexible space structure can be obtained by using a combination of a relatively low vision sample rate and a small number of structure-mounted accelerometers.

Chapter 4 presented the experimental validation of the fused estimation approach. Experiments were performed on the Robotic Team Interactive Microgravity System in the MIT Field and Space Robotics Laboratory. These studies paralleled the simulation results. Estimator performance was tested for various sensor configurations. It was found that when only using a single type of measurement, 6 accelerometers or a vision sample rate of 27 Hz is required to achieve an accurate estimate of the shape of the flexible structure. However, if the two sensor types are used together, an accurate estimate could be achieved with a limited vision sample rate of 9 hertz and three accelerometers.

5.2 Suggestions for Future Work

This thesis presented an approach to estimate the shape and dynamic parameters of a vibrating large space structure using remote vision sensors and structure-mounted accelerometers. There are many avenues for interesting research that would be natural extensions of this work.

This thesis considered the use structure-mounted accelerometers and remote vision sensors to estimate the shape and dynamic parameters of a large space structure. There are many more types of sensors such as strain gauges that may be useful in the estimation of these structures. The addition of these sensors to this estimation algorithm would a natural extension to this work.

Simple models of sensors were assumed in this study since the primary focus was to evaluate the effectiveness of the fusion-based approach. Though the performance of the models was based on realistic components, the models neglected drift, temperature variance, and bias. These factors could be substantial in a space system. These constraints could be added to the models to test the sensitivity and robustness of the algorithm for more realistic systems.

This style of analysis could be used as a design tool to determine the sensor configuration for a large space structure. In order to do this a cost function could be developed. This cost function could incorporate factors such as price, weight, reliability, power requirements, etc. to determine the least expensive configuration that meets the design specification.

There are a number of implementation issues that would provide interesting avenues for future research. In this thesis it was assumed that time-delays would be negligible. It was also assumed that the relative time between the vision and acceleration measurements is well known. In reality, this might not be the case. An interesting topic

for future research would be to determine the effects of these time-delays and methods to compensate for them. Also, this thesis has not considered where the computation would be completed. The computations could be performed on the structure, on the remote vision sensor, or on the control robots. Determining the where the estimation takes place and determining the flow of the information could be an interesting topic for further research.

In the experimental work presented in this thesis, all of the estimation was performed offline. However, in order use the estimator in the feedback loop to perform real-time control the estimation will need to be performed on-line. This on-line implementation could be performed on the Robotic Team Interactive Microgravity System in the MIT Field and Space Robotics Laboratory. This would also allow for experimental validation of the cooperative control approach for the transportation of large space structures presented in Section 3.4.

1   Andrisani, D. and C Gau. "Estimation using a Multirate Filter," *IEEE Transactions on Automatics Control*, Vol. 32, No. 7, pp. 653-656, July 1997.

2   Armesto, L., S. Chroust, M. Vincze, and J Tornero. "Multi-rate Fusion with Vision and Inertial Sensors," *Proceedings of the 2004 IEEE International Conference on Robotics and Automation (ICRA 2004)*, New Orleans, LA, April 2004.

3   Balas, G. J., and J. C. Doyle. "Identification of Flexible Structures for Robust Control," *IEEE Control Systems Magazine*, pp. 51-58, June 1990.

4   Bayard, B. S., F. Y. Hadaegh, and D. R. Meldrum. "Optimal Experiment Design for Identification of Large Space Structures," *Automatica*, Vol. 24, No. 3, pp. 357-364, 1998.

5   Bostelman, R., J. Albus, N. Dagalakis, A. Jacoff, and J. Gross, "Applications of the NIST RoboCrane," 5th *International Symposium on Robotics and Manufacturing*, Maui, HI, August 1994.

6   Brown, R.G., and P.Y.C. Hwang. *Introduction to Random Signals and Applied Kalman Filtering*, 3rd Ed. New York: John Wiley & Sons, 1997.

7   Chen C.-W., Huang, J.-K., Phan, M. and J.-N. Juang, "Integrated system identification and state estimation for control of flexible space structures," *Journal of Guidance, Control and Dynamics*, Vol. 15, No. 1, pp. 88 – 95, Jan-Feb 1992.

8   Chroust, S. G., and M. Vincze. "Fusion of Vision and Inertial Data for Motion and Structure Estimation," *Journal of Robotic Systems*, Vol. 21, No. 2, pp. 73-83, 2004.

9   Doggett, W. "Robotic Assembly of Truss Structures for Space Systems and Future Research Plans," *IEEE Aerospace Conference*, Big Sky, MT, March 2002.

10   Gawronski, W. *Dynamics and Control of Structures: A Modal Approach*, New York: Springer, 1998.

11   Gawronski, W. "Actuator and Sensor Placement for Structural Testing and Control," *Journal of Sound and Vibration*, Vol. 208, No. 1, pp. 101-109, November 1997.

12   Hac, A., and L. Liu. "Sensor and Actuator Location in Motion Control of Flexible Structures," *Journal of Sound and Vibration*, Vol. 167, No. 2, pp. 239-261, 1993.

13   Ishijima, Y., D. Tzeranis, and S. Dubowsky. "On-Orbit Maneuvering of Large Space Flexible Structures by Free-Flying Robots," *8th International Symposium on Artificial Intelligence, Robotics and Automation in Space, i-SAIRAS*, Munich, Germany, September 2005.

14   Juang, J., and R. S. Pappa. "An Eigensystem Realization Algorithm for Modal Parameter Identification and Model Reduction," *Journal of Guidance, Control and Dynamics,* Vol. 8, No. 5, pp. 620-627, 1985.

15   Julier, S.J., and J.K. Uhlmann. "A New Extension of the Kalman Filter to Nonlinear Systems," *Proceedings of AeroSense: The 11th International Symposium on Aerospace/Defense Sensing, Simulation and Controls,* Orlando, Florida, 1997.

16   Kar, I.N., K. Seto, and F. Doi. "Multimode Vibration Control of a Flexible Structure Using H∞-Based Robust Control," *IEEE/ASME Transactions on Mechatronics,* Vol. 5, No. 1, March 2000.

17   Kammer, D. C. and L. Yao. "Enhancement of On-Orbit Modal Identification of Large Space Structures Through Sensor Placement," *Journal of Sound and Vibration,* Vol. 171, No. 1, pp. 119-139, March 1994.

18   Lee, D.J. and M Tomizuka. "Multirate Optimal State Estimation with Sensor Fusion," *Proceedings of the American Control Conference,* Denver, Colorado, June 2003.

19   Lichter, M.D. and S. Dubowsky. "Shape, Motion, and Parameter Estimation of Large Flexible Space Structures using Range Images," *Proceedings of the 2005 IEEE International Conference on Robotics and Automation (ICRA 2005),* Barcelona, Spain, April 2005.

20   Lichter, M. D., S. Dubowsky, H. Ueno, and S. Mitani. "Shape, Motion and Parameter Estimation of Flexible Space Structures using Laser Range Finders," *Proceedings of Robotics: Science and Systems,* Cambridge, MA, June 2005.

21   Lichter, M. D. "Shape, Motion, and Inertial Parameter Estimation of Space Objects using Teams of Cooperative Vision Sensors," Ph.D. Thesis, Department of Mechanical Engineering, Massachusetts Institute of Technology, Cambridge, Massachusetts, 2004.

22   Lim, K. B. "Disturbance Rejection Approach to Actuator and Sensor Placement," *Journal of Guidance, Control and Dynamics,* Vol. 20, No. 1, pp. 202-204, 1997.

23   Lim, K.B., P.G. Maghami, and S.M Joshi. "Comparison of Controller Designs for an Experimental Flexible Structure," *IEEE Control Systems Magazine,* Vol. 12, No. 3, pp. 108–118, June 1992.

24   Lively, P. S., M. J. Attalla, and N. W. Hagood. "Dynamic Shape Estimation using Kalman Filtering," *Proceedings of SPIE, Vol. 3985: Smart Structures and Materials,* N. M. Wereley ed., pp. 521-532, 2000.

25   Maghami, P.G. and S.M. Joshi. "Sensor/Actuator Placement for Flexible Space Structures," *IEEE Trans. on Aerospace and Electronic Systems,* Vol. 29, No. 2, pp. 345-351, April 1993.

References

26   Mankins, J.C. "A Fresh Look at Space Solar Power: New Architectures, Concepts and Technologies," *Proceedings of the 38th International Astronautical Federation Conference*, 1997.

27   Mankins, J. C., "A Technical Overview of the "Sun Tower" Solar Power Satellite Concept," *Acta Astronautica*, Vol. 50, No. 6, March 2002, pp 369-377.

28   Mangalgiri, V. "Analysis for the Robotic Assembly of Large Flexible Space Structures," Master's Thesis, Department of Mechanical Engineering, Massachusetts Institute of Technology, Cambridge, Massachusetts, 2004.

29   Metaxas, D., D. Terzopoulis. "Shape and Nonrigid Motion Estimation through Physics-Based Synthesis," *IEEE Transactions on Pattern Analysis and Machine Intelligence*, Vol. 15, No. 6, June 1993.

30   Niwa, S., T. Masuda, and Y. Sezaki. "Kalman Filter with Time-variable Gain for a Multisensor Fusion System," *Proceedings of the 1999 IEEE International Conference on Multisensor Fusion and Integration for Intelligent Systems*, Taipei, Taiwan, August 1999.

31   Oda, M., H. Ueno, and M. Mori. "Study of the Solar Power Satellite in NASDA," *Proceedings of the 7th International Symposium on Artificial Intelligence, Robotics, and Automation in Space: i-SAIRAS 2003*, NARA, Japan, May 2003.

32   Rehbinder, H. and B. K. Ghosh. "Multi-Rate Fusion of Visual and Inertial Data," Proceedings of the *IEEE Conference on Multisensor Fusion and Integration of Intelligent Systems*, Baden-Baden, Germany, 2001.

33   "SICK LMS 200 Technical Description," [online document], Available HTTP: http://www.sick.com/us/news/archive/listing/lmssensors/en.html

34   Sim, E., and S. W. Lee. "Active Vibration Control of Flexible Structures with Acceleration Feedback," *Journal of Guidance, Control, and Dynamics*, Vol. 16, No. 2, pp. 413-415, 1993.

35   Sims, C. S., and J, Juang. "Reduced-Order Filtering for Flexible Space Structures," *First IEEE Conference on Control Applications*, pp. 183-187, September 1992.

36   "Space Solar Power Systems Brochure," [online document], Available HTTP: http://www.ista.jaxa.jp/res/b05/ssps/03.html

37   Staritz, P.J., S. Skaff, C. Urmson, and W. Whittaker. "Skyworker: A Robot for Assembly, Inspection and Maintenance of Large Scale Orbital Facilities," *Proceedings of the 2001 IEEE International Conference on Robotics and Automation (ICRA 2001)*, Seoul, Korea, pp. 4180-4185, May 2001.

38   Tongco, E. and D. Meldrum. "Optimal Sensor Placement of Large Flexible Space Structures," *Journal of Guidance, Control, and Dynamics*, Vol. 19, No. 4, pp. 961-963, 1996.

39   Tse, D. N. C. and G. R. Heppler. "Shape Determination for Large Flexible Satellites via Stereo Vision," *Journal of Spacecraft and Rockets*, Vol. 29, No. 1, pp. 108-117, 1992.

40   Tzeranis, D. "Manipulation of Flexible Structural Modules by Space Robots During LSS Construction," Master's Thesis, Department of Mechanical Engineering, Massachusetts Institute of Technology, Cambridge, Massachusetts, 2005.

41   Udwadia, F. E. "Methodology for Optimum Sensor Locations for Parameter Identification in Dynamic Systems," *Journal of Engineering Mechanics*, Vol. 120, No. 2, February 1994.

42   Ueno, H., T. Nishimaki, M. Oda, and N. Inaba. "Autonomous Cooperative Robots for Space Structure Assembly and Maintenance," *Proceedings of the 7th International Symposium on Artificial Intelligence, Robotics, and Automation in Space: i-SAIRAS 2003*, NARA, Japan, May 2003.

43   Wakabayashi, Y., Y. Ohkami, M. Miyata, T. Adachi, and T. Iijima. "A Compact Laser Range Finder for Space Applications," *Proceedings of SPIE, Vol. 3714: Enabling Photonic Technologies for Aerospace Applications*, A.R. Pirich, E.W. Taylor, eds., pp. 131-138, 1999.

44   Williams, T. and G. Slater, "Steady-State Matched Model Reduction for Flexible Structures with Acceleration Measurements," *Journal of Guidance, Control, and Dynamics*, Vol. 28, No. 2, pp. 360-363, March-April 2005.

45   Williams, T., "Identification of Large Space Structures: A Factorization Approach," *Journal of Guidance, Control, and Dynamics*, Vol. 10, No. 5, pp. 466-473, 1987.

46   Yao, L., W. A. Sethares and D. C. Kammer. "Sensor Placement for On-orbit Modal Identification of Large Space Structure via a Genetic Algorithm," *IEEE International Conference on Systems Engineering*, September 1992.

47   Zhang, H.-H. and H.-X. Wu. "Identifiability of Flexible Space Structures," *Proceedings of the IEEE Conference on Decision and Control*, Vol. 2, pp. 1488-1493, Dec. 1993.

A

MODAL DECOMPOSITION OF ACCELERATION MEASUREMENTS

In the special case that the modal frequencies are well known and the structure is very lightly damped, it is possible to perform a modal decomposition on the acceleration measurements. This appendix presents the modifications to the estimator for this case. The acceleration can be defined at any point on the structure using:

$$\ddot{z}(x,t) = \sum_{i=1}^{m} \phi_i(x)\ddot{q}_i(t) = \Phi(x)\ddot{\mathbf{q}}(t) \tag{A.1}$$

where the unforced dynamics of $q(t)$ are given by:

$$\ddot{q}_i(t) = -\omega_i^2 q_i(t) - 2\zeta_i \omega_i \dot{q}_i(t)$$

The acceleration measurements are made in a time-invariant sample space $X \subset S$. These acceleration measurements can be written as:

$$
\begin{Bmatrix} \bar{\bar{z}}(x_1,t) \\ \vdots \\ \bar{\bar{z}}(x_k,t) \\ \vdots \\ \bar{\bar{z}}(x_n,t) \end{Bmatrix} = \begin{Bmatrix} \ddot{z}(x_1,t) \\ \vdots \\ \ddot{z}(x_k,t) \\ \vdots \\ \ddot{z}(x_n,t) \end{Bmatrix} + \begin{Bmatrix} e_{a,1} \\ \vdots \\ e_{a,k} \\ \vdots \\ e_{a,n} \end{Bmatrix}
$$

where $\ddot{z}(x_k,t)$ is the true acceleration at sample point x_k, $\overline{\ddot{z}}(x_k,t)$ is the measured acceleration at x_k, and $e_{a,k}$ is the measurement noise at x_k. Rewriting this equation in vector form gives:

$$\overline{\ddot{z}} = \ddot{z} + \mathbf{e_a}$$

Substituting in $\ddot{z}$ from Equation (A.1) allows $\overline{\ddot{z}}$ to be expressed in terms of the modal coefficients as:

$$\overline{\ddot{z}} = \Phi\ddot{q} + \mathbf{e_a}$$
$$= -\Phi\left(\Omega^2 q + 2\Omega Z\dot{q}\right) + \mathbf{e_a}$$

where Ω is a diagonal matrix containing the modal frequencies and Z is a diagonal matrix containing the modal damping coefficients. If $Z \ll \Omega$, the damping term can be neglected and we can arrive at a coarse estimate of modal coefficients using:

$$\breve{q}_a = -\left(M_x\Omega^2\right)^{-1}\left\langle \Phi,\overline{\ddot{z}} \right\rangle_x \tag{A.2}$$

where M_x is the modal correlation matrix defined over the sample space X. However this estimate will have a time varying bias. This can be seen by evaluating the error expectation. The error is given by:

$$\mathbf{e_q} = \breve{q}_a - q$$
$$= -\left(M_x\Omega^2\right)^{-1}\left\langle \Phi,\overline{\ddot{z}} \right\rangle_x - q$$
$$= -\left(M_x\Omega^2\right)^{-1}\Phi^T\left\{-\Phi\left(\Omega^2 q + 2\Omega Z\dot{q}\right) + \mathbf{e_a}\right\} - q$$
$$= 2\Omega^{-1}Z\dot{q} - \left(M_x\Omega^2\right)^{-1}\left\langle \Phi,\mathbf{e_a} \right\rangle_x$$

Since $\mathbf{e}_a$ is zero mean, the expected value of the error is:

$$E[\tilde{\mathbf{q}}_a - \mathbf{q}] = 2E[\,\Omega^{-1}Z\mathbf{q}\,]$$

In this case, the measurement error covariance for the is given by:

$$
\begin{aligned}
\Lambda_{aa} &= E\!\left[(\tilde{q}-q)(\tilde{q}-q)^T\right] \\
&= E\!\left[\left(2\Omega^{-1}Z\mathbf{q}+\left(M_x\Omega^2\right)^{-1}\langle\Phi,\mathbf{e}_a\rangle_x\right)\!\left(2\Omega^{-1}Z\mathbf{q}+\left(M_x\Omega^2\right)^{-1}\langle\Phi,\mathbf{e}_a\rangle_x\right)^T\right]
\end{aligned}
$$

Since we assume that Ω is known and damping is negligible, the measurement covariance becomes:

$$
\begin{aligned}
\Lambda_{aa} &= E\!\left[\left(\left(M_x\Omega^2\right)^{-1}\langle\Phi,\mathbf{e}_a\rangle_x\right)\!\left(\left(M_x\Omega^2\right)^{-1}\langle\Phi,\mathbf{e}_a\rangle_x\right)^T\right] \\
&= \left(M_x\Omega^2\right)^{-1}E\!\left[\Phi^T\mathbf{e}_a\left(\Phi^T\mathbf{e}_a\right)^T\right]\!\left(M_x\Omega^2\right)^{-1} \\
&= \Omega^{-2}M_x^{-1}\Phi^T E\!\left[\mathbf{e}_a\mathbf{e}_a^T\right]\!\Phi\,\Omega^{-2}M_x^{-1} \\
&= \sigma_a^2\Omega^{-2}M_x^{-1}M_x\Omega^{-2}M_x^{-1} \\
&= \sigma_a^2\Omega^{-4}M_x^{-1}
\end{aligned}
\qquad\text{(A.3)}
$$

where σ_a^2 is the variance on the accelerometer measurements. It is assumed that all accelerometers have the same measurement variance. The estimator can now be implemented as explained in Chapter 2. This technique is suboptimal, but if there are a large amount of accelerometers, this step could greatly reduce the computational burden of the algorithm.

B

UNCERTAINTY IN MODE SHAPES

The simulations presented in this thesis all used perfect knowledge of the mode shapes. In reality, the mode shapes will likely be uncertain due to modeling errors, parameter uncertainty, nonlinearities, etc. In [21], Dr. Matthew Lichter showed that imperfect modal knowledge degrades the estimator performance gracefully. This section studies the effect of this uncertainty in simulation.

These simulations study the effect of errors in the a priori knowledge of the mode shapes for free-free beam. The estimator is formulated using a baseline structural model. This baseline model is the same structure described in Section 3.2.1. A second model of the structure is generated by placing lumped masses at the ends of the beam. This model is simulated in MATLAB and provides measurements to the Kalman filter.

The sensor configuration implemented in these simulations uses measurements from 8 optimally placed accelerometers and a 5 Hz vision sample rate. This configuration meets the specification laid out in Section 3.2.2. As before, Gaussian white noise is added to sensor measurements, details on the magnitude of the noise can be found in Section 3.2.1.

The magnitude of the added mass is varied to observe how the errors in the mode shapes affect the estimator performance. Figure B.1 shows the change in the modal coefficients for a 50 kg mass added at each end of the flexible structure. The uncertainty in the modal frequencies also increases with the additional mass. Some sample values are found in Table B.1.
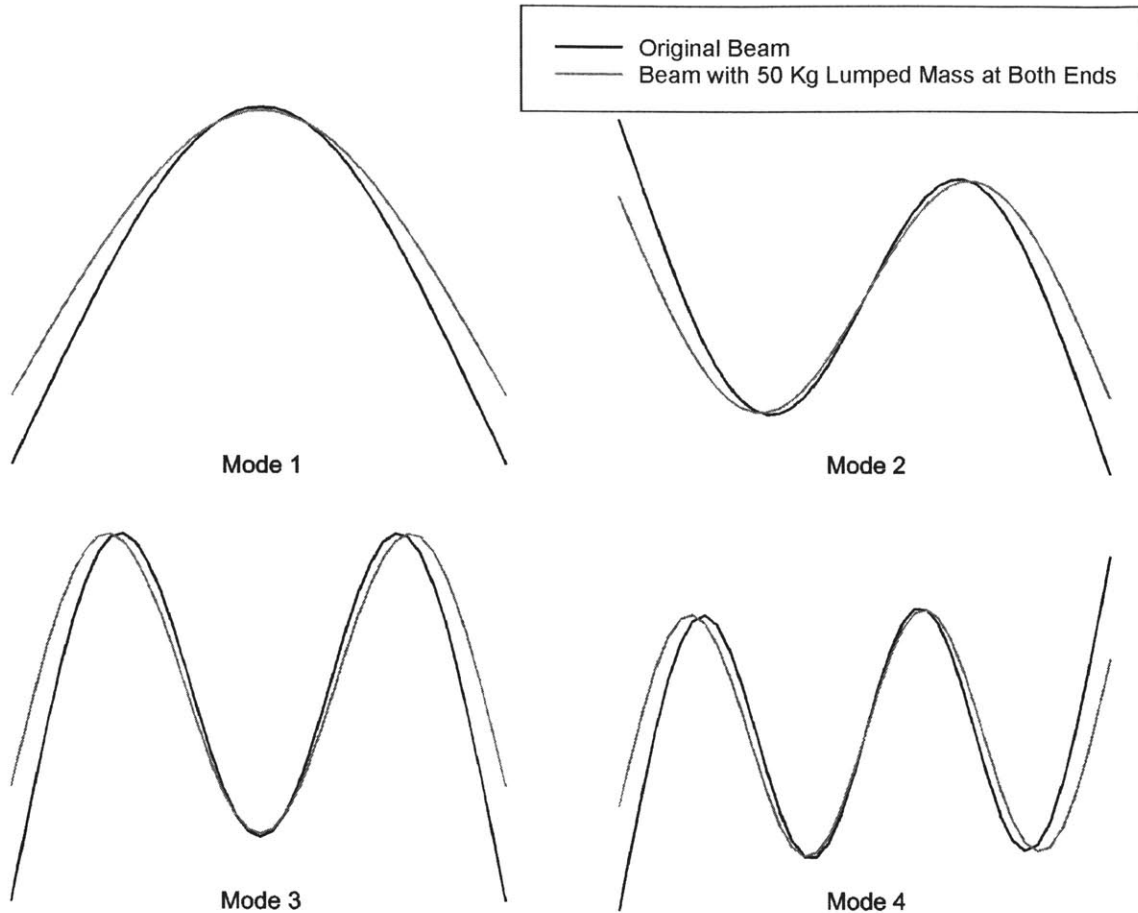
Figure B.1. Changes in mode shapes for 50 kg lumped masses.

Each perturbed configuration is tested against 20 different data sets in order to ensure independence on initial conditions. In each data set, all modes are vibrating with equal energy. The phase for each mode, φ_i, was randomly selected over the interval from 0 to 2π. In order to have a steady state final condition, the structure damping is set to zero. A total of 14 modes were simulated, 8 of these modes were estimated.

Table B.1. Frequency changes for lumped mass at the beam ends.

	Original Beam	Beam with 50 kg lump masses	Beam with 100 kg lump masses
Mode 1	0.185 Hz	0.147 Hz	0.130 Hz
Mode 2	0.510 Hz	0.422 Hz	0.391 Hz
Mode 3	1.001 Hz	0.851 Hz	0.809 Hz
Mode 4	1.655 Hz	1.437 Hz	1.387 Hz

A sample estimated and actual first modal coefficient for the case when the simulated structure has 50 kg lumped masses on each end is shown in Figure B.2. The estimated modal coefficient vibrates with lower amplitude. This is due to the properties of a Kalman filter.
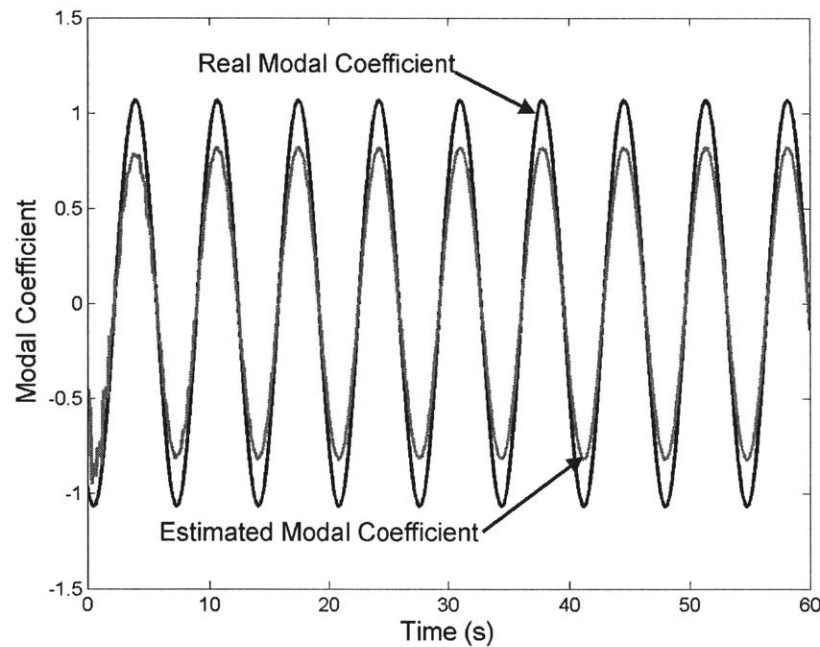

Figure B.2. Estimated and actual first modal coefficient for a simulated structure with 50 kg lumped masses using knowledge of free-free mode shapes.

A Kalman filter provides an estimate that minimizes covariance between the estimated and actual state. The mode shapes used in the process model (shown in Figure

B.1) have a larger magnitude at the beam-ends. Hence, the lower amplitude modal coefficient reduces the estimated error at the beam-ends. However, the error at the end the beam, see Figure B.3, does not go to zero. This is due to the properties of the mode shapes at the center of the structure. Figure B.1 shows that although the additional mass decreases the magnitude of the modal shapes at the beam-ends, they remain virtually identical at the center. Therefore, the smaller amplitude vibrations decrease the error at the beam-ends but increase the error at the middle of the structure, shown in Figure B.4. The Kalman filter determines the amplitude that minimizes the covariance between the estimated and actual state.
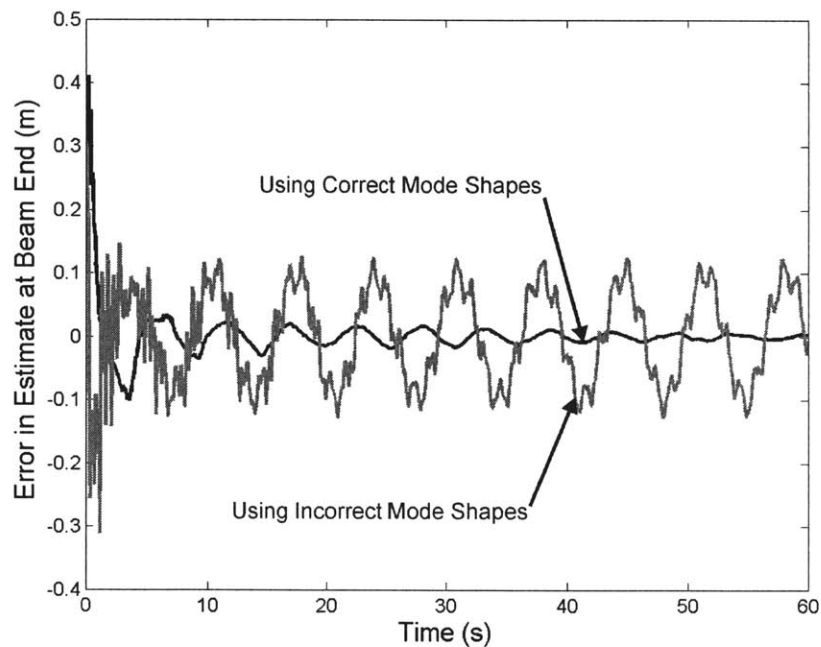

Figure B.3. Error in shape estimate at beam-end when simulating a structure with 50 kg lumped masses using knowledge of free-free mode shapes.
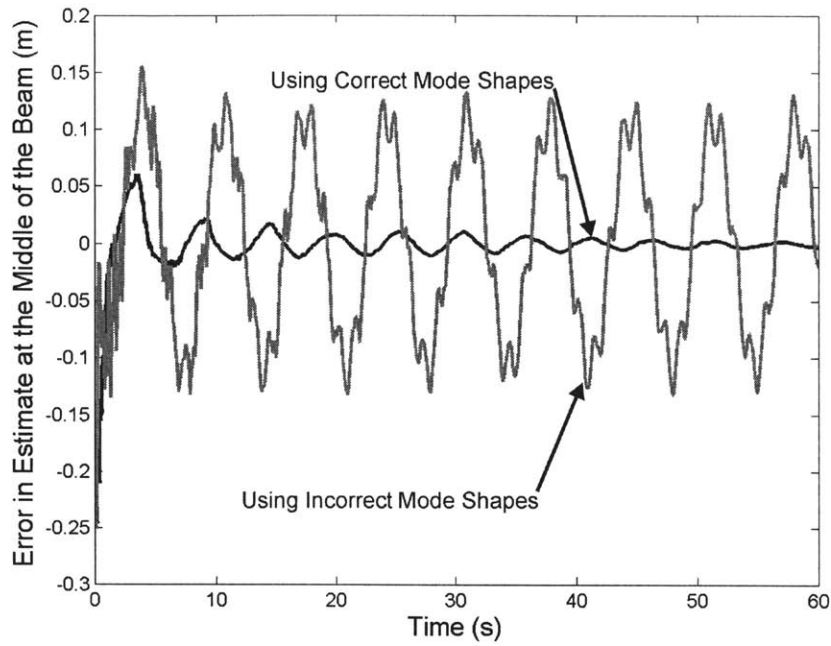
Figure B.4. Error in shape estimate at middle of the beam when simulating a structure with 50 kg lumped masses using knowledge of free-free mode shapes.

Figure B.5 summarizes the results of the mode shape simulations. The maximum shape error at the beam has a nearly linear relation to the amount of lumped mass added. As was predicted by the analytical analysis in [21], the estimator performance degrades gracefully as modal uncertainty increases.
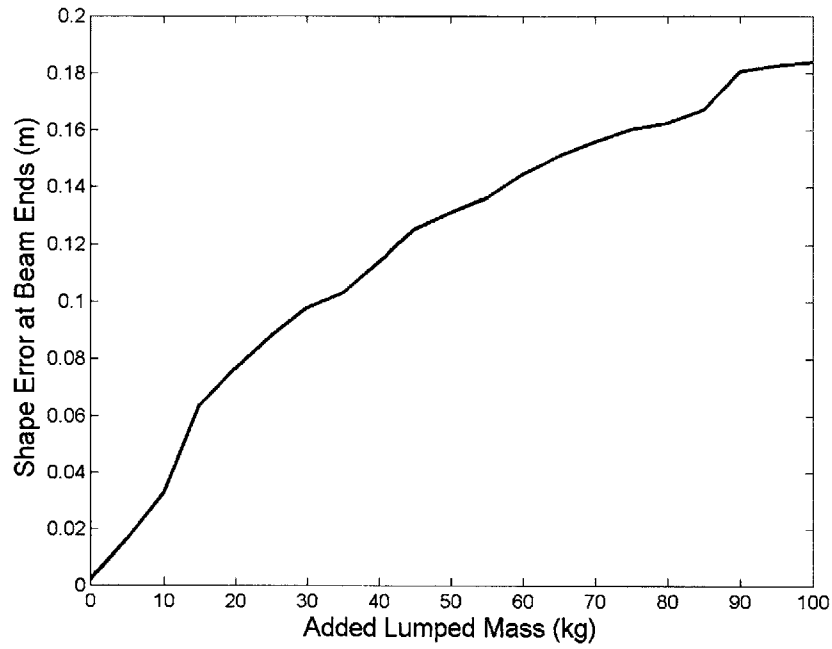
Figure B.5. Maximum error at beam-ends for converged estimate vs. amount of lumped mass added to the structure.

APPENDIX

C

DERIVATION OF DISCRETE-TIME PROCESS MODEL

This appendix presents the derivation of the discrete-time process model for a flexible structure. The dynamics of a flexible structure in modal coordinates can be written as:

$$\ddot{\mathbf{q}} + 2\Omega Z \dot{\mathbf{q}} + \Omega^2 \mathbf{q} = \mathbf{BF} \tag{C.1}$$

where Ω is a diagonal matrix of the modal frequencies, Z is the modal damping matrix and B is the input matrix. This model can be put into state space form as follows:

$$\begin{bmatrix} \dot{q}_i \\ \ddot{q}_i \end{bmatrix} = \begin{bmatrix} 0 & 1 \\ -\omega_i^2 & -2\zeta_i\omega_i \end{bmatrix} \begin{bmatrix} q_i \\ \dot{q}_i \end{bmatrix} + \begin{bmatrix} 0 \\ b_i \end{bmatrix} F \tag{C.2}$$

where b_i is a row vector containing the magnitudes of the mode shapes at the locations of the actuators.

The model can be rewritten in discrete-time. The form of this model is given by:

$$x_{k+1} = A_d x_k + B_d F_k$$

where A_d and B_d are given by:

$$A_d = e^{A\Delta t}, \quad B_d = \int_0^{\Delta t} e^{A\tau} B \, d\tau$$

There are many ways to compute the matrix exponential. Here we diagonalize the matrix. The eigenvalues and eigenvectors of the A matrix were found to be:

$$\lambda_{1,2} = -\omega_i \zeta_i \pm i\omega_{d,i}, \quad v_{1,2} = \begin{bmatrix} 1 \\ -\omega_i \zeta_i \pm i\omega_{d,i} \end{bmatrix}$$

Then the state transition matrix can be found using:

$$e^{A\Delta t} = M \begin{bmatrix} exp((\omega_i\zeta_i + i\omega_{d,i})\Delta t) & 0 \\ 0 & exp((\omega_i\zeta_i - i\omega_{d,i})\Delta t) \end{bmatrix} M^{-1}$$

where the columns of M are given by the eigenvectors. Performing the indicated matrix multiplications and simplifying gives the state transition matrix.

$$e^{A\Delta t} = exp(-\zeta_i\omega_i\Delta t) \begin{bmatrix} \dfrac{\omega_i\zeta_i}{\omega_{d,i}} sin(\omega_{d,i}\Delta t) + cos(\omega_{d,i}\Delta t) & \dfrac{1}{\omega_{d,i}} sin(\omega_{d,i}\Delta t) \\ -\dfrac{\omega_i^2}{\omega_{d,i}} sin(\omega_{d,i}\Delta t) & cos(\omega_{d,i}\Delta t) - \dfrac{\omega_i\zeta_i}{\omega_{d,i}} sin(\omega_{d,i}\Delta t) \end{bmatrix} \quad (C.3)$$

Now we will derive the discrete input matrix B_d. The input matrix is given by:

$$B_d = \int_0^{\Delta t} e^{A\tau} B \, d\tau$$

Substituting in the state transition matrix and B from equation (C.2) leaves:

$$B_d = \int_0^{\Delta t} exp(-\zeta_i\omega_i\tau) \begin{bmatrix} \dfrac{\omega_i\zeta_i}{\omega_{d,i}} sin(\omega_{d,i}\tau) + cos(\omega_{d,i}\tau) & \dfrac{1}{\omega_{d,i}} sin(\omega_{d,i}\tau) \\[2ex] -\dfrac{\omega_i^2}{\omega_{d,i}} sin(\omega_{d,i}\tau) & cos(\omega_{d,i}\tau) - \dfrac{\omega_i\zeta_i}{\omega_{d,i}} sin(\omega_{d,i}\tau) \end{bmatrix} \begin{bmatrix} 0 \\ b_i \end{bmatrix} d\tau$$

$$= \int_0^{\Delta t} exp(-\zeta_i\omega_i\tau) \begin{bmatrix} \dfrac{b_i}{\omega_{d,i}} sin(\omega_{d,i}\tau) \\[2ex] b_i\left\{ cos(\omega_{d,i}\tau) - \dfrac{\omega_i\zeta_i}{\omega_{d,i}} sin(\omega_{d,i}\tau) \right\} \end{bmatrix} d\tau$$

Performing the integration leaves:

$$B_d = \begin{bmatrix} b_i\left(\dfrac{exp(-\zeta_i\omega_i\Delta t)}{\omega_i^2}\left(-\dfrac{\omega_i}{\omega_{d,i}} sin(\omega_{d,i}\Delta t) - cos(\omega_{d,i}\Delta t) \right) + \dfrac{1}{\omega_i^2} \right) \\[3ex] b_i\dfrac{exp(-\zeta_i\omega_i\Delta t)}{\omega_{d,i}} sin(\omega_{d,i}\Delta t) \end{bmatrix} \qquad (C.4)$$

If the state is expanded to include ω_i and ζ_i, the discrete-time process model becomes:

$$\begin{Bmatrix} q_i \\ \dot{q}_i \\ \omega_i \\ \zeta_i \end{Bmatrix}_{(t+\Delta t)} = \begin{Bmatrix} exp(-\zeta_i\omega_i\Delta t)\left(q_i cos(\omega_{d,i}\Delta t) + \dfrac{\dot{q}_i + \zeta_i\omega_i q_i}{\omega_{d,i}} sin(\omega_{d,i}\Delta t) \right) \\ exp(-\zeta_i\omega_i\Delta t)\left(\dot{q}_i cos(\omega_{d,i}\Delta t) - \dfrac{\zeta_i\omega_i\dot{q}_i + \omega_i^2 q_i}{\omega_{d,i}} sin(\omega_{d,i}\Delta t) \right) \\ \omega_i \\ \zeta_i \end{Bmatrix}_{(t)}$$

$$+ \begin{Bmatrix} \displaystyle\sum_{k=1}^{p} b_{ki}F_k\left(\dfrac{exp(-\zeta_i\omega_i\Delta t)}{\omega_i^2}\left(-\dfrac{\omega_i}{\omega_{d,i}} sin(\omega_{d,i}\Delta t) - cos(\omega_{d,i}\Delta t) \right) + \dfrac{1}{\omega_i^2} \right) \\ \displaystyle\sum_{k=1}^{p} \dfrac{b_{ki}F_k\, exp(-\zeta_i\omega_i\Delta t)}{\omega_{d,i}} sin(\omega_{d,i}\Delta t) \\ 0 \\ 0 \end{Bmatrix}_{(t)}$$